FFI RAPPORT

Observation modelling and detection probability for space-based AIS reception - Extended observation area

HØYE Gudrun

FFI/RAPPORT-2004/04390

Observation modelling and detection probability for space-based AIS reception - Extended observation area

HØYE Gudrun

FFI/RAPPORT-2004/04390

FORSVARETS FORSKNINGSINSTITUTT
Norwegian Defence Research Establishment
P O Box 25, NO-2027 Kjeller, Norway

FORSVARETS FORSKNINGSINSTITUTT (FFI)
Norwegian Defence Research Establishment

P O BOX 25
N0-2027 KJELLER, NORWAY

UNCLASSIFIED

SECURITY CLASSIFICATION OF THIS PAGE (when data entered)

REPORT DOCUMENTATION PAGE

1) PUBL/REPORT NUMBER	2) SECURITY CLASSIFICATION	3) NUMBER OF PAGES
FFI/RAPPORT-2004/04390	UNCLASSIFIED	56
1a) PROJECT REFERENCE	**2a) DECLASSIFICATION/DOWNGRADING SCHEDULE**	
FFI-III/1002/913	-	

4) TITLE

OBSERVATION MODELLING AND DETECTION PROBABILITY FOR SPACE-BASED AIS RECEPTION - Extended observation area

5) NAMES OF AUTHOR(S) IN FULL (surname first)

HØYE Gudrun

6) DISTRIBUTION STATEMENT

Approved for public release. Distribution unlimited. (Offentlig tilgjengelig)

7) INDEXING TERMS

IN ENGLISH:	IN NORWEGIAN:
a) AIS	a) AIS
b) Ship detection	b) Skipsdeteksjon
c) Detection probability	c) Deteksjonssannsynlighet
d) Observation modelling	d) Observasjonsmodellering
e) Space-based surveillance	e) Rombasert overvåking

THESAURUS REFERENCE:

8) ABSTRACT

This report evaluates the performance with respect to ship detection probability for a space-based AIS system. The report continues the work of a previous report that studied the ship detection probability for space-based AIS for swath widths up to 800 nm. This report extends the analyses to include also fields of view to the horizon (2880 nm wide swath).

An observation model for the space-based AIS system has been established, and software for the simulations has been developed in Matlab. Analytical expressions for the ship detection probability have also been derived.

The analyses show that a single AIS sensor in Low Earth Orbit could handle up to 900 ships within the field of view with a ship detection probability of better than 99%. A global constellation of AIS sensors could handle up to 2000 ships with an update rate of twice per day.

9) DATE	AUTHORIZED BY	POSITION
	This page only	
2005-09-20	Johnny Bardal	Director

UNCLASSIFIED

SECURITY CLASSIFICATION OF THIS PAGE (when data entered)

ISBN- 978-82-464-1312-9

CONTENTS

APPENDIX

Observation modelling and detection probability for space-based AIS reception - Extended observation area

1 INTRODUCTION

The Universal Shipborne Automatic Identification System (AIS) is a ship-to-ship and ship-to-shore reporting system based on broadcasting of short messages in the maritime VHF band. The AIS messages could possibly also be received from space, as illustrated in Figure 1.1. However, a space-based AIS sensor would see a much larger area on the ground than the AIS system is designed for, and as a result simultaneous reception of AIS messages could occur. The content of such simultaneous AIS messages would be lost.

A previous report (1) studied the feasibility of space-based AIS reception with respect to ship detection probability for swath widths up to 800 nm. This report extends the analyses to include ship detection probability modelling and simulations for fields of view to the horizon. For an AIS receiver at 600 km altitude this corresponds to a 2880 nm wide swath.

Chapter 2 gives an overview of the AIS system, while Chapter 3 presents the observation model that has been developed for the statistical analyses. The results are presented in Chapter 4 and discussed in Chapter 5. A summary is given in Chapter 6. The software that was developed for the simulations is described in a separate report (5).

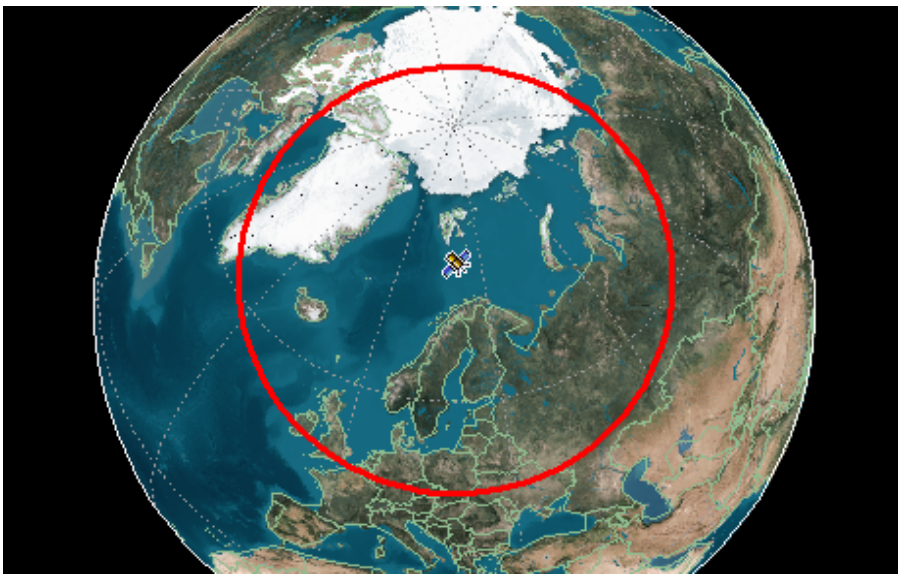

Figure 1.1 *A space-based concept for AIS reception. The red circle indicates the AIS sensor's field of view to horizon from 600 km altitude.*

2 THE AIS SYSTEM

2.1 The AIS concept

AIS is a ship-to-ship and ship-to-shore reporting system developed for the safety of navigation at sea and for maritime traffic monitoring purposes. The ships are broadcasting information such as identity, position, heading, etc. to neighbouring ships and shore stations within reach. Figure 2.1 illustrates the AIS concept.

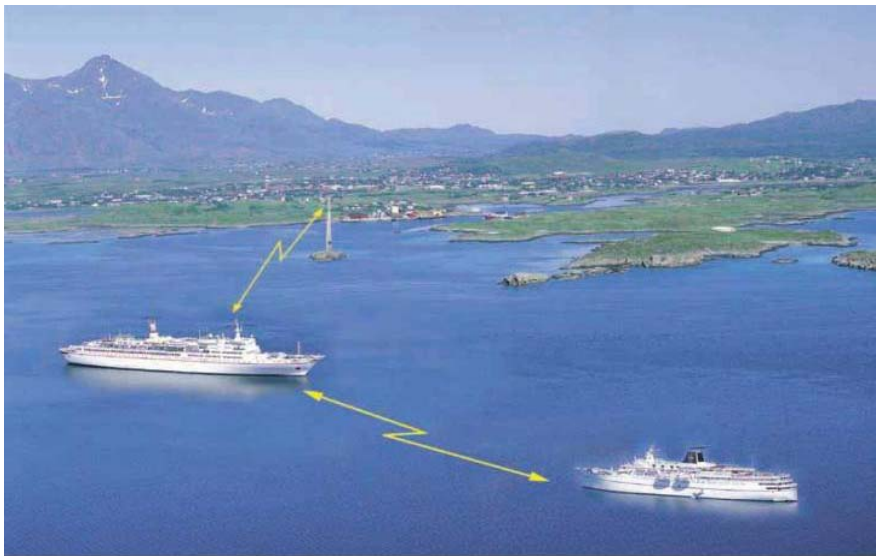

Figure 2.1 The AIS ship-to-ship and ship-to-shore concept. (Courtesy of Kongsberg Seatex, Norway).

AIS is mandatory on the following ships:

- All passenger ships
- All cargo ships from 500 GT and upwards not engaged on international voyages
- All ships from 300 GT and upwards engaged on international voyages

The installation is to be completed by 1. July 2008. Details regarding the implementation plan and the ships that are required to carry AIS are given in Regulation 19 of Chapter V of the International Convention for the Safety of Life at Sea (SOLAS) (2).

2.2 The AIS messages

Four different message categories are used in the AIS system. Table 2.1 shows the four categories together with a list of their contents and required reporting interval.

Message category	Message contents	Reporting interval
Static messages	Ship IMO number, call sign & name, length & beam, etc.	6 min
Dynamic messages	Ship position, time, course over ground, speed over ground, heading, etc.	As given in Table 2.2
Voyage related messages	Destination, cargo type, waypoints, etc.	6 min
Safety related messages	-	As required

Table 2.1 The different message categories that are used in the AIS-system.

Dynamic messages	
Ship's dynamic conditions	**Reporting interval**
Ship at anchor or moored and not moving faster than 3 knots	3 min
Ship at anchor or moored and moving faster than 3 knots	10 s
Ship 0-14 knots	10 s
Ship 0-14 knots and changing course	3 1/3 s
Ship 14-23 knots	6 s
Ship 14-23 knots and changing course	2 s
Ship > 23 knots	2 s
Ship > 23 knots and changing course	2 s

Table 2.2 Reporting intervals for dynamic messages.

2.3 The AIS reporting system

The AIS reporting system is based on the broadcasting of digital messages using the Time Division Multiple Access (TDMA) communication technology. The messages are entered into a 1 minute long message frame of 2250 message slots. The message entry is synchronized to the universal time coordinated (UTC), and the length of each message is limited to 256 bits. The two VHF maritime mobile channels 87B (AIS1) and 88B (AIS2) are allocated to the AIS. Messages are broadcasted alternately on the two channels giving the system a total capacity of 4500 message slots per minute.

A mobile AIS station gains access to the AIS network by using the RATDMA (Random Access), ITDMA (Incremental), and SOTDMA (Self-Organizing) access schemes, ref. (3). The TDMA technology provides for automatic contention resolution, it makes the radio link robust, and communications integrity is maintained even in overload situations. Figure 2.2 illustrates the ITDMA principle.

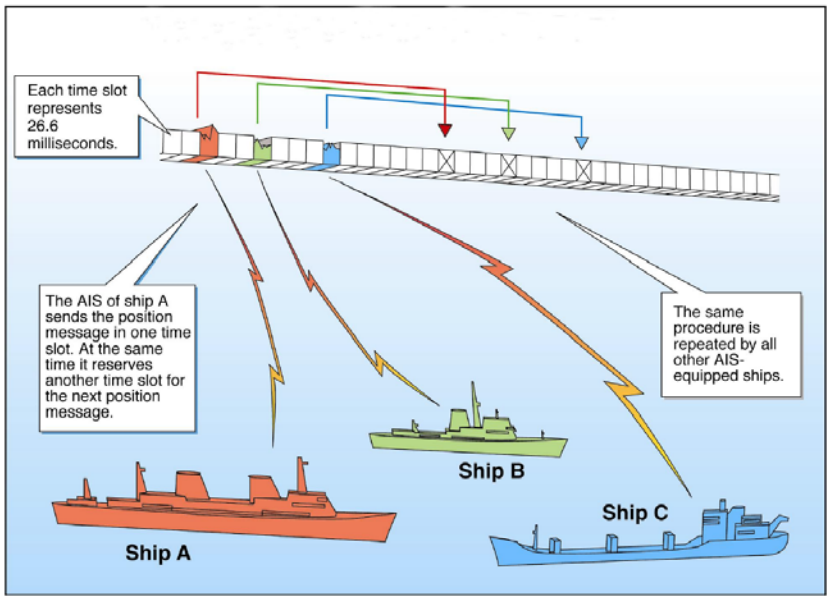

Figure 2.2 The AIS ITDMA principle.

2.4 The SOTDMA access scheme

SOTDMA will be the access scheme normally used on the open oceans. The purpose of the SOTDMA access scheme is to offer an access algorithm which quickly resolves conflicts without intervention from controlling stations. Figure 2.3 illustrates the SOTDMA access scheme. A description of the most important SOTDMA parameters is given below. Note that this is a simplified description of the SOTDMA access scheme. The AIS system uses two independent channels for transmission, where the ships transmit alternately on each of the two channels. To simplify the modelling we have assumed that the ships transmit on only one channel. For a complete description of the system, see Section 3.3.4-3.3.5 in (3).

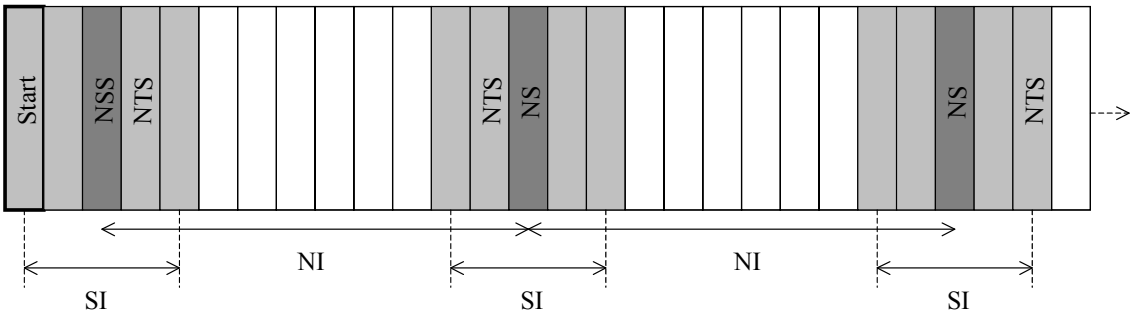

Figure 2.3 The SOTDMA access scheme.

At power on, an AIS station monitors the TDMA channel for one minute to determine channel activity, other participating member IDs, current slot assignments, and reported positions of other users. The station then enters the network and starts to transmit reports according to its own schedule.

The first slot used by a station to announce itself on the data link is called the Nominal Start Slot (NSS). Other repeatable transmissions are generally selected with the NSS as reference.

The Nominal Slot (NS) is used as the centre around which slots are selected for transmission of reports. For the first transmission in a frame, the NSS and NS are equal. The NS is given by

$$NS = NSS + n \cdot NI, \qquad (0 < n < Rr) \tag{2.1}$$

where n is an integer, Rr is the Report rate, i.e., the number of position reports per frame, and NI is the Nominal Increment.

The Report rate relates to the reporting interval ΔT as follows

$$Rr = \frac{60}{\Delta T} \tag{2.2}$$

The Nominal Increment is given in number of slots and is found from

$$NI = 2250 / Rr = 37.5 \cdot \Delta T \tag{2.3}$$

where 2250 is the number of slots per frame (= 1 minute).

The Selection Interval (SI) is the collection of slots that can be candidates for position reports. It is centred around the Nominal Slot, and covers the interval

$$SI = \{NS - 0.1NI, NS + 0.1NI\} \tag{2.4}$$

Finally, the Nominal Transmission Slot (NTS) is the slot used for the transmission. The Nominal Transmission Slot is chosen within the Selection Interval.

A summary of the parameters is given in Table 2.3.

Name	Symbol	Description	Equation	Min value	Max value
Nominal Start Slot	NSS	The first slot used by a station to announce itself on the data link.	-	0	2249
Nominal Slot	NS	The centre around which slots are selected for transmission of position reports.	(2.1)	0	2249
Report Rate	Rr	Number of position reports per frame.	(2.2)	1/3	30
Nominal Increment	NI	The distance (number of slots) between two Nominal Slots.	(2.3)	75	6750
Selection Interval	SI	The collection of candidate slots for position reports.	(2.4)	$0.2NI$	$0.2NI$
Nominal Trans-mission Slot	NTS	The slot used for transmission.	-	0	2249

Table 2.3 The SOTDMA parameters.

2.5 The AIS communication range

The communication range of a mobile AIS station is limited by the local horizon and the AIS transmitter power to about 20 nm. AIS communication areas can then be partly overlapping or next to each other as shown in Figure 2.4.

In Figure 2.4 ship A communicates with no other ships, while ship B communicates with ship C, and ship C communicates with ships B, D, and F, etc. Ship C will have to organize its reporting with ships B, D, and F, while ship D will have to get organized also with ship E. Ship E will further have to get organized with the shore station. When more ships enter the picture the organizing gets more complex. The SOTDMA scheme is, however, designed to handle a large number of ships. In the event of an overload situation, the AIS stations have the ability to reduce their communication range, thereby giving priority to collision avoidance for the closest ships.

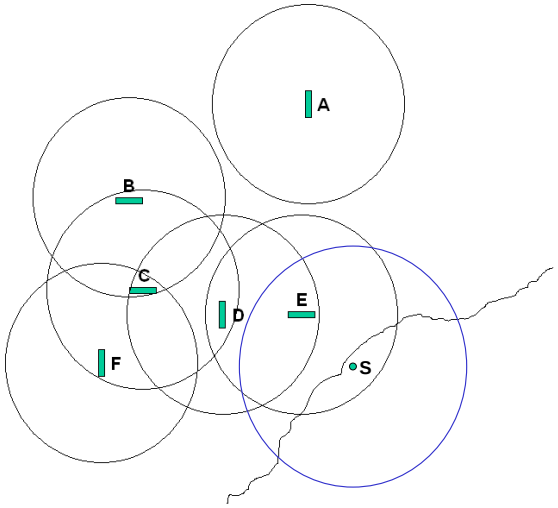

Figure 2.4 *Communication range (circles) for individual ships, within which the TDMA organizes the AIS reporting. The radius of each ship (A-F) circle is about 20 nm, and somewhat bigger for an elevated ground station (S).*

3 OBSERVATION MODEL

An observation model has been developed in order to evaluate the performance of the space-based AIS concept with respect to ship detection probability for a field of view to the horizon. Based on the observation model, the system performance has been evaluated through computer simulations. The software for the simulations has been developed in Matlab version 7 and can be found in a separate report (5). Analytical expressions for the ship detection probability have also been developed.

3.1 General considerations

3.1.1 Organized areas

The reporting between ships within communication range is organized by the TDMA-algorithm using the SOTDMA access scheme to avoid coinciding transmissions. From space, the AIS sensor will see more than one such area, as illustrated in Figure 3.1. To be able to analyse the situation, we have defined what we call an *organized area*. Within an organized area all AIS transmissions are organized to avoid coinciding transmissions, while ships in different organized areas are assumed to transmit independently of each other.

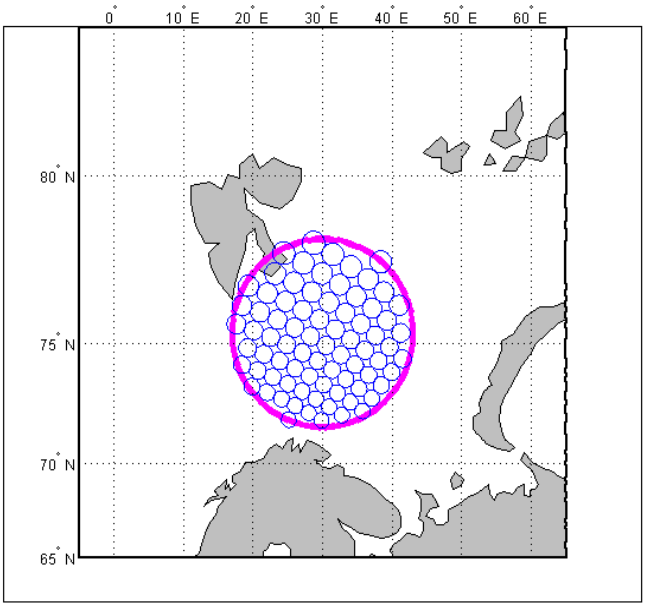

Figure 3.1 Illustration showing organized areas as small blue circles and the AIS sensor's field of view as a big red circle. In this example, the AIS sensor covers a 400 nm wide area on the ground.

3.1.2 Observation area and number of ships

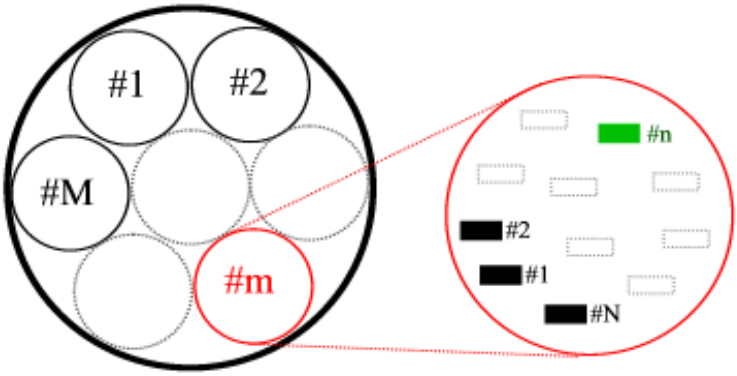

Figure 3.2 The observation area with M organized areas. Detail shows organized area $\#m$ with N ships.

Figure 3.2 shows an observation area containing a total of M organized areas. Each organized area contains a number of ships N^m, where m indicates organized area $\#m$. Ship $\#n$ in organized area $\#m$ transmits with a ship reporting interval denoted ΔT_n^m.

The total number of ships N_{tot} within the observation area is

$$N_{tot} = \sum_{m=1}^{M} N^m \tag{3.1}$$

3.1.3 Maximum possible number of ships within an organized area

The maximum possible number of ships within an organized area is given by

$$N_{\max} = n_{ch} \cdot \frac{2250}{Rr} = 37.5 \cdot n_{ch} \cdot \Delta T \tag{3.2}$$

where n_{ch} is the number of independent channels that are used for the transmissions, 2250 is the number of slots per frame (=1 minute), and Rr is the Report rate given by Equation (2.2). We have assumed that all ships within the organized area transmit with the same Report rate. Table 3.1 shows the maximum possible number of ships within an organized area for different ship reporting intervals ΔT when the number of independent channels is $n_{ch} = 2$.

Ship reporting interval	Max number of ships
2 s	150
6 s	450
10 s	750
3 min	13 500

Table 3.1 Maximum possible number of ships within an organized area for different ship reporting intervals when two independent channels are used for the transmissions.

3.1.4 Two mechanisms for coinciding transmissions

The emission of AIS messages is synchronised to UTC, and the allocation of message slots is coordinated within each organized area. A space-based AIS sensor will see many organized areas within its field of view, and the possibility of simultaneous reception of AIS messages arises. The content of simultaneously received AIS messages, hereafter referred to as coinciding transmissions, will be lost.

There are two possible mechanisms for coinciding transmissions:

1. The AIS messages are sent in the same message slot from different organized areas.
2. The AIS messages are sent in different message slots from different organized areas, but are received simultaneously due to different signal path lengths.

The AIS standard uses a distance delay buffer in the AIS messages to prevent overlap between messages that are sent in adjacent timeslots as long as the difference in the signal path length is less than 202 nm. For a nadir-pointing AIS sensor at 600 km altitude this translates into a ground range of 394 nm relative to nadir, see Figure 3.3. This means that for swath widths up to about 800 nm only the first mechanism for coinciding transmissions is effective. For swath widths larger than 800 nm the second mechanism for coinciding transmissions must also be included in the analyses.

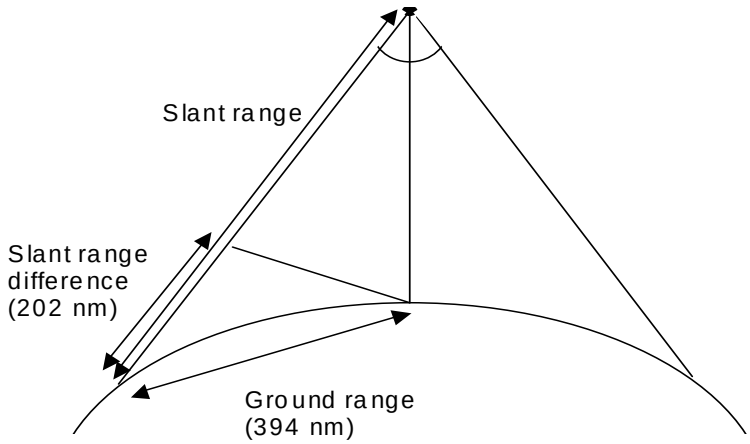

Figure 3.3 Geometry showing the relation between the slant range difference and the corresponding ground range for an AIS sensor at 600 km altitude.

In a previous report (1), only the first mechanism for coinciding transmissions was included in the analyses, limiting the swath width to 800 nm. In the present report also the second mechanism for coinciding transmissions is included in the observation modelling and subsequent analyses, extending the possible field of view to the horizon.

3.2 Observation geometry

Figure 3.4 shows the observation geometry for the system as viewed from the side and from above. The parameters used in the figure have the following meaning; H_{sat} is the AIS sensor's altitude, R_s is the slant range from the AIS sensor to the organized area being observed (marked by red circle), $R_s^{horizon}$ is the slant range distance to the horizon, $R_s^{\max}$ is the slant range distance to the outer edge of the observation area ($R_s^{\max} \le R_s^{horizon}$), and $\Delta R_s = 202$ nm is the maximum slant range difference allowed by the distance delay buffer.

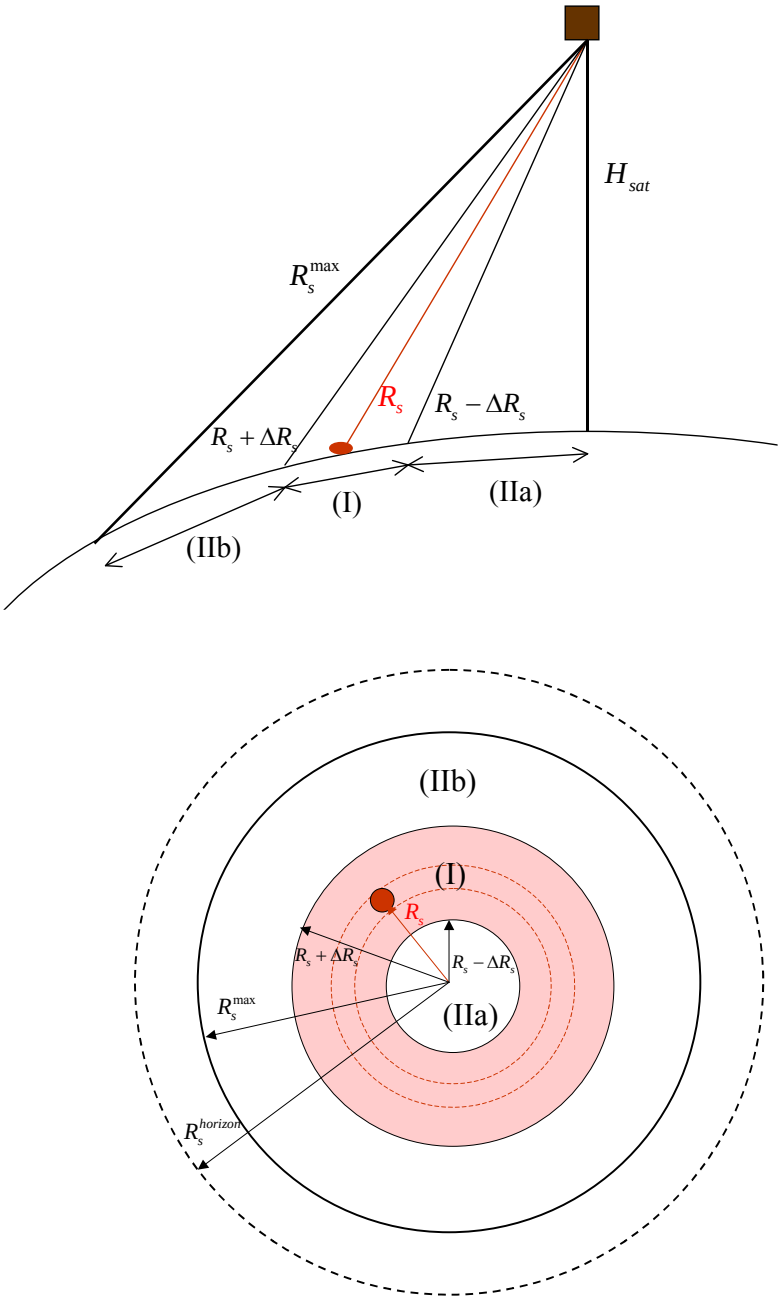

Figure 3.4 The observation geometry for the system. The upper figure shows the system viewed from the side. In the lower figure the system is viewed from above.

Main area (I) (marked by pink in the figure) contains the organized area being observed and all other organized areas that the AIS sensor receives transmissions from within the distance delay buffer relative to that organized area.

Main area (IIa) contains all the organized areas that the AIS sensor receives transmissions from outside the distance delay buffer relative to the organized area being observed, and that arrives at the AIS sensor too early.

Main area (IIb) contains all the organized areas that the AIS sensor receives transmissions from outside the distance delay buffer relative to the organized area being observed, and that arrives at the AIS sensor too late.

3.3 Observation area

Figure 3.5 shows the observation area for an AIS sensor at 600 km altitude with field of view to the horizon. To simplify the calculations, we have assumed that the observation area is *quadratic*. Each small square in the figure represents one organized area of size 40×40 nm. The total observation area consists of 5184 (72×72) organized areas and is 2880 nm wide.

Imagine now that we make quadratic frames with thickness corresponding to one organized area (40 nm). An example of such a quadratic frame is shown in Figure 3.5 (marked by red). Starting at the centre of the observation area, the first quadratic frame consists of 4 organized areas and is labelled frame #1. The next frame consists of 12 organized areas and is labelled frame #2. We continue labelling frames until reaching the outer edge of the observation area. For an AIS sensor at 600 km altitude with field of view to the horizon, the observation area consists of a total of 36 such frames.

For the ship detection probability calculations we assume that the slang range distance to each organized area within a frame is the same. This is true for a circular observation area with circular frames, and can be used as a good approximation also for a quadratic observation area with quadratic frames.

The total number of organized areas M^l in frame $\#l$ is given by

$$M^l = 4 \cdot (2l - 1) \tag{3.3}$$

while the total number of organized areas M in an observation area that contains l frames is given by

$$M = 4l^2 \tag{3.4}$$

The total numbers of organized areas M_I^l and M_{II}^l that are found within main areas (I) and (II) respectively as seen from frame $\#l$ are given by

$$M_I^l = \sum_{j=\min L_I^l}^{\max L_I^l} M^j$$
$$M_{II}^l = \sum_{j=\min L_{IIa}^l}^{\max L_{IIa}^l} M^j + \sum_{j=\min L_{IIb}^l}^{\max L_{IIb}^l} M^j \qquad (3.5)$$

where $\min L_I^l$ and $\max L_I^l$ are the minimum and maximum frame numbers for main area (I) as seen from frame $\#l$, $\min L_{IIa}^l$ and $\max L_{IIa}^l$ are the minimum and maximum frame numbers for main area (IIa) as seen from frame $\#l$, $\min L_{IIb}^l$ and $\max L_{IIb}^l$ are the minimum and maximum frame numbers for main area (IIb) as seen from frame $\#l$, and M^j is given by Equation (3.3).

Table A.1-Table A.7 in Appendix A give the values for the parameters that are relevant for the ship detection probability calculations.

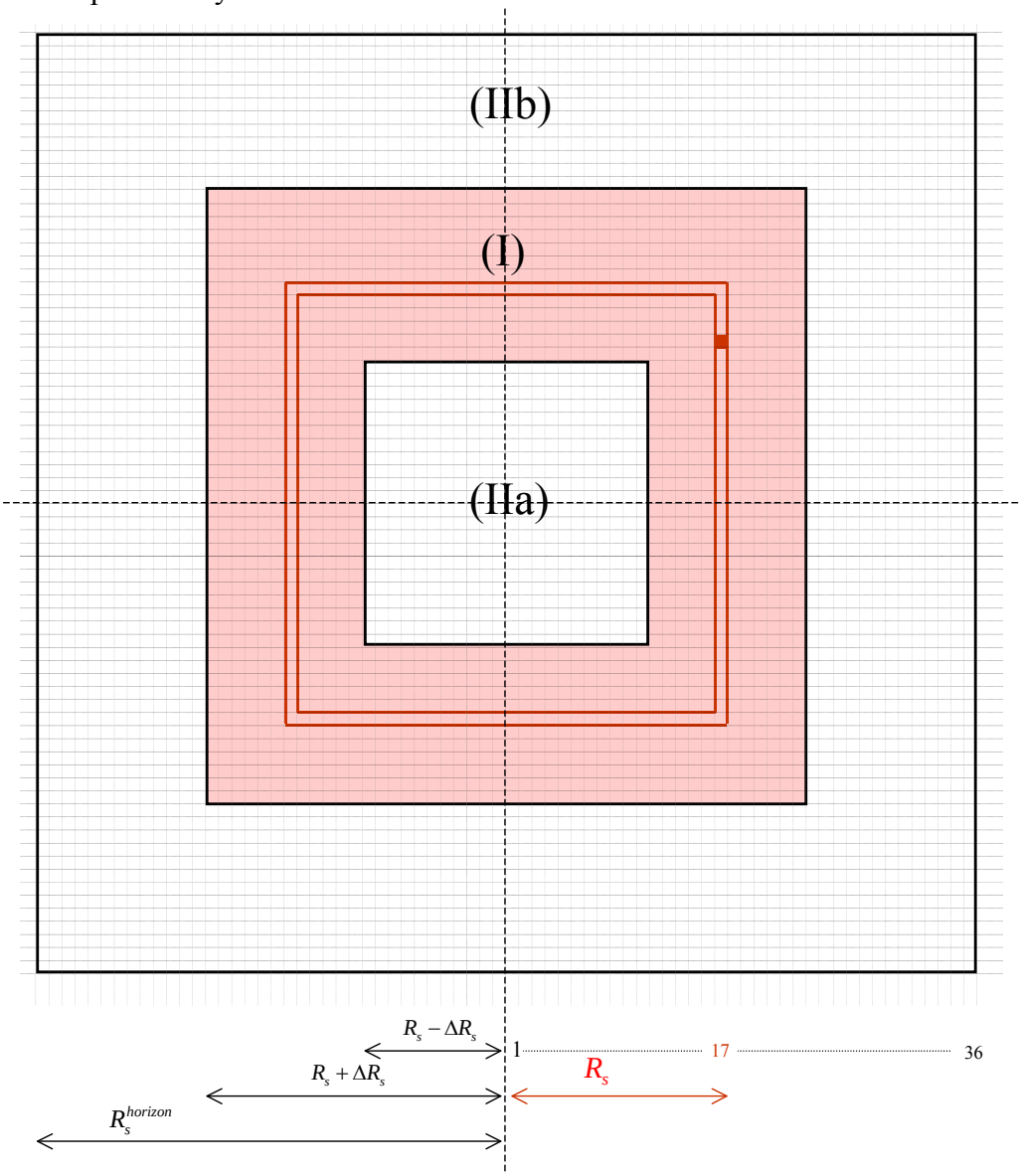

Figure 3.5 The quadratic observation area for an AIS sensor at 600 km altitude with field of view to the horizon.

3.4 Assumptions

For the simulations and calculations the following assumptions have been made:

1) The number of ships within each organized area is the same, that is:

$$N^m = N \tag{3.6}$$

for all $m = 1, 2, \ldots M$. The total number of ships within the observation area is then given by

$$N_{tot} = \sum_{m=1}^{M} N^m = N \cdot M \tag{3.7}$$

2) The ship reporting interval is the same for all ships in all organized areas, that is:

$$\Delta T_n^m = \Delta T \tag{3.8}$$

for all $n = 1, 2, \ldots N$, $m = 1, 2, \ldots M$.

3) The observation area is quadratic.

3.5 Simulations

The simulation program is described in a separate report (5). The following algorithm has been applied for the simulations:

1) Assign Nominal Transmission Slots (NTS) to all ships within an organized area. Each slot is picked randomly within the corresponding Selection Interval in such a way that there are no coinciding transmissions.

2) Repeat step 1 for all organized areas within the observation area.

3) Based on this, calculate the number of detected ships within the observation area, taking into consideration both mechanisms for coinciding transmissions.

4) Repeat step 1-3 a given number of times (statistical trial).

5) Calculate the mean value for the number of detected ships and the corresponding ship detection probability.

Parameters used as input for the simulations are:

- Number of organized areas, M
- Number of ships within each organized area, N
- Ship reporting interval, ΔT
- Observation time, T_{obs}

In addition, information about the observation geometry is given in a separate input file.

3.6 Analytical approach

We have also developed analytical expressions for the ship detection probability.

3.6.1 The nominal ship detection probability equation

We will first derive the nominal ship detection probability equation.

The probability $p_{\Delta T}$ that a given ship's transmission does *not coincide* with the transmission from any ship in one (arbitrarily chosen) of the other organized areas during an observation time $T_{obs} = \Delta T$, where ΔT is the ship reporting interval, is given by

$$p_{\Delta T}^{I} = 1 - \frac{N}{N_{\max}} = 1 - \frac{N_{tot}}{37.5 \cdot n_{ch} \cdot M \cdot \Delta T} \tag{3.9}$$

if the organized area is placed in main area (I) relative to the ship being observed, and by

$$p_{\Delta T}^{II} = 1 - k \cdot \frac{N}{N_{\max}} = 1 - k \cdot \frac{N_{tot}}{37.5 \cdot n_{ch} \cdot M \cdot \Delta T} \tag{3.10}$$

if the organized area is placed in main area (IIa) or (IIb) relative to the ship being observed. Here N is the number of ships within each organized area, $N_{\max}$ is the maximum possible number of ships within an organized area as given by Equation (3.2), M is the total number of organized areas within the observation area, N_{tot} is the total number of ships within the observation area as given by Equation (3.7), $n_{ch} = 2$ is the number of independent channels used for the transmissions, and the fill factor k is given by

$$k = k\left(\tfrac{N}{N_{\max}}\right) = 2 - \frac{N}{N_{\max}} = 2 - \frac{N_{tot}}{37.5 \cdot n_{ch} \cdot M \cdot \Delta T} \tag{3.11}$$

and is described in Appendix B.

For $N \ll N_{\max}$, i.e., when there are only a few ships within each organized area

$$k \to 2 \tag{3.12}$$

while for $N \to N_{\max}$, i.e., when each organized area is almost filled with ships

$$k \to 1 \tag{3.13}$$

and

$$p_{\Delta T}^{II} \to p_{\Delta T}^{I} \tag{3.14}$$

The probability ${}_m p_{\Delta T}^{M}$ that the transmission from a ship in organized area $\#m$ does *not coincide* with the transmission from any ship in any of the other M organized areas in the observation area during an observation time $T_{obs} = \Delta T$ is given by

$$ {}_m p_{\Delta T}^{M} = \left(p_{\Delta T}^{I} \right)^{M_I^m - 1} \cdot \left(p_{\Delta T}^{II} \right)^{M_{II}^m} = \left(1 - \frac{N_{tot}}{37.5 \cdot n_{ch} \cdot M \cdot \Delta T} \right)^{M_I^m - 1} \cdot \left(1 - k \cdot \frac{N_{tot}}{37.5 \cdot n_{ch} \cdot M \cdot \Delta T} \right)^{M_{II}^m} \tag{3.15} $$

where M_I^m is the number of organized areas in main area (I) as seen from organized area $\#m$, M_{II}^m is the number of organized areas in main areas (IIa) and (IIb) as seen from organized area $\#m$, and

$$ M_I^m + M_{II}^m = M \tag{3.16} $$

for all $m = 1, ..., M$.

The *nominal* ship detection probability P_n for an arbitrary ship within the observation area during an observation time T_{obs} can then be written

$$ \begin{aligned} P_n &= 1 - \left(1 - {}_m p_{\Delta T}^{M} \right)^{\frac{T_{obs}}{\Delta T}} \\ &= 1 - \left[1 - \frac{1}{M} \sum_{m=1}^{M} \left(1 - \frac{N_{tot}}{37.5 \cdot n_{ch} \cdot M \cdot \Delta T} \right)^{M_I^m - 1} \cdot \left(1 - k \cdot \frac{N_{tot}}{37.5 \cdot n_{ch} \cdot M \cdot \Delta T} \right)^{M_{II}^m} \right]^{\frac{T_{obs}}{\Delta T}} \end{aligned} \tag{3.17} $$

For observation areas that are small enough that only one mechanism for coinciding transmissions is effective (swath widths less than 800 nm for a nadir-pointing AIS sensor at 600 km altitude) we have

$$ \begin{aligned} M_I^m &= M \\ M_{II}^m &= 0 \end{aligned} \tag{3.18} $$

and the nominal ship detection probability equation (3.17) reduces to

$$ p_n = 1 - \left[1 - \left(1 - \frac{N_{tot}}{37.5 \cdot n_{ch} \cdot M \cdot \Delta T} \right)^{M-1} \right]^{\frac{T_{obs}}{\Delta T}} \tag{3.19} $$

which is equivalent to Equation (3.19) in (1).

3.6.2 The average ship detection probability equation

The *average* ship detection probability P_a for an arbitrary ship within the observation area during the observation time T_{obs} is given by

$$P_a = 1 - \left[1 - \left(1 - \frac{N_{tot}}{37.5 \cdot n_{ch} \cdot M \cdot \Delta T} \right)^{\bar{M}_I - 1} \cdot \left(1 - k \cdot \frac{N_{tot}}{37.5 \cdot n_{ch} \cdot M \cdot \Delta T} \right)^{\bar{M}_{II}} \right]^{\frac{T_{obs}}{\Delta T}} \tag{3.20}$$

where the fill factor k is given by Equation (3.11) and

$$\begin{aligned} \bar{M}_I &= \frac{1}{M} \sum_{m=1}^{M} M_I^m \\ \bar{M}_{II} &= \frac{1}{M} \sum_{m=1}^{M} M_{II}^m \end{aligned} \tag{3.21}$$

Here M_I^m is the number of organized areas in main area (I) as seen from organized area $\#m$, M_{II}^m is the number of organized areas in main areas (IIa) and (IIb) as seen from organized area $\#m$, and

$$\bar{M}_I + \bar{M}_{II} = M \tag{3.22}$$

Values for $\bar{M}_I$, $\bar{M}_{II}$, and M are given in Table A.7 in Appendix A.4.

For observation areas that are small enough that only one mechanism for coinciding transmissions is effective (swath widths less than 800 nm for a nadir-pointing AIS sensor at 600 km altitude), the average ship detection probability equation (3.20) reduces to Equation (3.19), i.e., in this case the average and the nominal ship detection probability equations are identical.

3.6.3 The independent ship detection probability equation

We will now derive the independent ship detection probability equation.

The average fraction s of ships in main areas (IIa) and (IIb) as seen from an arbitrary ship within the observation area can be calculated from

$$s = s(H_{sat,} \Delta S) = \frac{\bar{M}_{II}}{M} \tag{3.23}$$

Note that s, hereafter referred to as the overlap factor, depends on both the AIS sensor altitude H_{sat} and the swath width ΔS. Values for s can be found in Table A.7 in Appendix A.4.

The number of organized areas M can now be eliminated from the ship detection probability equation (3.20) by setting

$$M = N_{tot} \tag{3.24}$$

This corresponds to assuming that all ships transmit independently of each other since each organized area now contains only one ship.

Substituting Equation (3.24) into Equations (3.11), (3.22), and (3.23) gives

$$\begin{aligned} \bar{M}_I &= (1-s)\cdot N_{tot} \\ \bar{M}_{II} &= s \cdot N_{tot} \end{aligned} \tag{3.25}$$

and

$$k = 2 - \frac{1}{37.5 \cdot n_{ch} \cdot \Delta T} \tag{3.26}$$

For $n_{ch} \cdot \Delta T \geq 2$ s Equation (3.26) can be approximated by

$$k = 2 \tag{3.27}$$

By substituting Equations (3.24), (3.25), and (3.27) into the average ship detection probability equation (3.20) the following expression for the *independent* ship detection probability P_i can be obtained

$$\boxed{P_i = 1 - \left[1 - \left(1 - \frac{1}{37.5 \cdot n_{ch} \cdot \Delta T} \right)^{(1-s)\cdot N_{tot} - 1} \cdot \left(1 - \frac{2}{37.5 \cdot n_{ch} \cdot \Delta T} \right)^{s \cdot N_{tot}} \right]^{\frac{T_{obs}}{\Delta T}}} \tag{3.28}$$

Equation (3.28) is a good approximation when $n_{ch} \cdot \Delta T \geq 2$ s , i.e., when $\Delta T \geq 1$ s (since $n_{ch} = 2$), and this will always be the case for the existing AIS system (see Table 2.2).

For observation areas that are small enough that only one mechanism for coinciding transmissions is effective (swath widths less than 800 nm for a nadir-pointing AIS sensor at 600 km altitude) we have

$$s = 0 \tag{3.29}$$

and the independent ship detection probability equation (3.28) reduces to

$$P_i = 1 - \left[1 - \left(1 - \frac{1}{37.5 \cdot n_{ch} \cdot \Delta T} \right)^{N_{tot}-1} \right]^{\frac{T_{obs}}{\Delta T}} \tag{3.30}$$

Note that Equation (3.30) is independent of both the AIS sensor altitude H_{sat} and the swath width ΔS, while Equation (3.28) depends on both these parameters through the overlap factor s. Equation (3.30) is further valid for both even and uneven ship distributions, while Equation (3.28) is only valid for even ship distributions.

3.6.4 The simplified ship detection probability equation

Finally, we will derive the simplified ship detection probability equation.

Two factors in the independent ship detection probability equation (3.28) can be simplified in the following way (4):

$$\left(1 - \frac{1}{37.5 \cdot n_{ch} \cdot \Delta T} \right)^{(1-s) \cdot N_{tot} - 1} = \exp\left(- \frac{(1-s) \cdot N_{tot} - 1}{37.5 \cdot n_{ch} \cdot \Delta T} \right) \tag{3.31}$$

and

$$\left(1 - \frac{2}{37.5 \cdot n_{ch} \cdot \Delta T} \right)^{s \cdot N_{tot}} = \exp\left(- \frac{2s \cdot N_{tot}}{37.5 \cdot n_{ch} \cdot \Delta T} \right) \tag{3.32}$$

when $n_{ch} \cdot \Delta T \geq 2$ s.

Substituting Equations (3.31) and (3.32) into the independent ship detection probability equation (3.28) gives the following expression for the *simplified* ship detection probability P_s

$$\boxed{P_s = 1 - \left[1 - \exp\left(- \frac{(1+s) \cdot N_{tot}}{37.5 \cdot n_{ch} \cdot \Delta T} \right) \right]^{\frac{T_{obs}}{\Delta T}}} \tag{3.33}$$

Equation (3.33) is a good approximation when $n_{ch} \cdot \Delta T \geq 2$ s, i.e., when $\Delta T \geq 1$ s (since $n_{ch} = 2$), and this will always be the case for the existing AIS system (see Table 2.2).

For observation areas that are small enough that only one mechanism for coinciding transmissions is effective (swath widths less than 800 nm for a nadir-pointing AIS sensor at 600 km altitude) we have

$$s = 0 \tag{3.34}$$

and the simplified ship detection probability equation (3.33) reduces to

$$P_s = 1 - \left[1 - \exp\left(-\frac{N_{tot}}{37.5 \cdot n_{ch} \cdot \Delta T} \right) \right]^{\frac{T_{obs}}{\Delta T}} \tag{3.35}$$

Note that Equation (3.35) is independent of both the AIS sensor altitude H_{sat} and the swath width ΔS, while Equation (3.33) depends on both these parameters through the overlap factor s. Equation (3.35) is further valid for both even and uneven ship distributions, while Equation (3.33) is only valid for even ship distributions.

4 RESULTS

Figure 4.1-Figure 4.14 present the results from the simulations and calculations.

The calculations have assumed that the AIS sensor has a field of view to the horizon. Corresponding values for AIS sensor altitude, swath width, and observation time are given in Table 4.1.

AIS sensor altitude, H_{sat}	**Swath width to horizon, ΔS_h**	**Observation time, T_{obs}**
400 km	2400 nm	617 s
600 km	2880 nm	772 s
800 km	3280 nm	919 s
1000 km	3600 nm	1049 s

Table 4.1 Corresponding values for AIS sensor altitude, swath width, and observation time for an AIS sensor with field of view to the horizon.

In some cases, swath widths that do not correspond to an AIS sensor field of view to the horizon have been used. The observation times can than be found from Table A.1 in Appendix A.1.

The simplified ship detection probability equation (3.33) has been used for the calculations unless otherwise is explicitly stated.

The different symbols appearing in Figure 4.1-Figure 4.14 have the following meaning:

H_{sat}	−	AIS sensor altitude
ΔS	−	Swath width
ΔT	−	Ship reporting interval
T_{obs}	−	Observation time
N_{tot}	−	Total number of ships within the observation area
# Trials	−	Number of stochastic trials used in the simulations
“1 coinc mech”	−	The simulations/calculations include only one mechanism for coinciding transmissions (see Section 3.1.4)
“2 coinc mech”	−	The simulations/calculations include both mechanisms for coinciding transmissions (see Section 3.1.4)
“Nominal”	−	The nominal ship detection probability equation (3.17)/(3.19)
“Average”	−	The average ship detection probability equation (3.20)/(3.19)
“Independent”	−	The independent ship detection probability equation (3.28)/(3.30)
“Simplified”	−	The simplified ship detection probability equation (3.33)/(3.35)

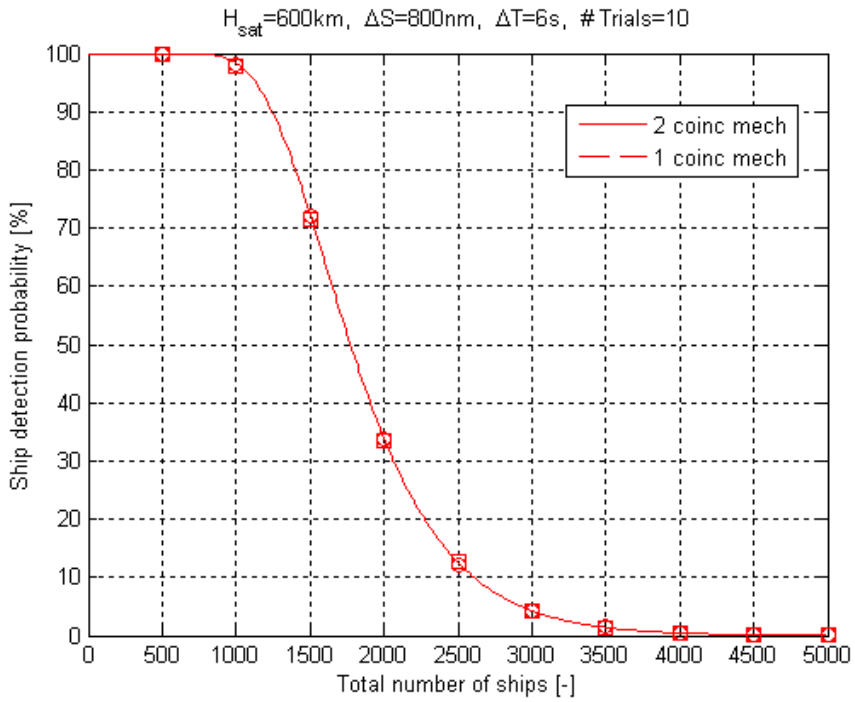

Figure 4.1 *Ship detection probability as a function of total number of ships within the observation area for an 800 nm wide swath. Circles and squares (2 and 1 coinciding mechanisms) show results from the simulations, while solid and dashed lines show corresponding results from calculations with the nominal ship detection probability equation (3.17)/(3.19).*

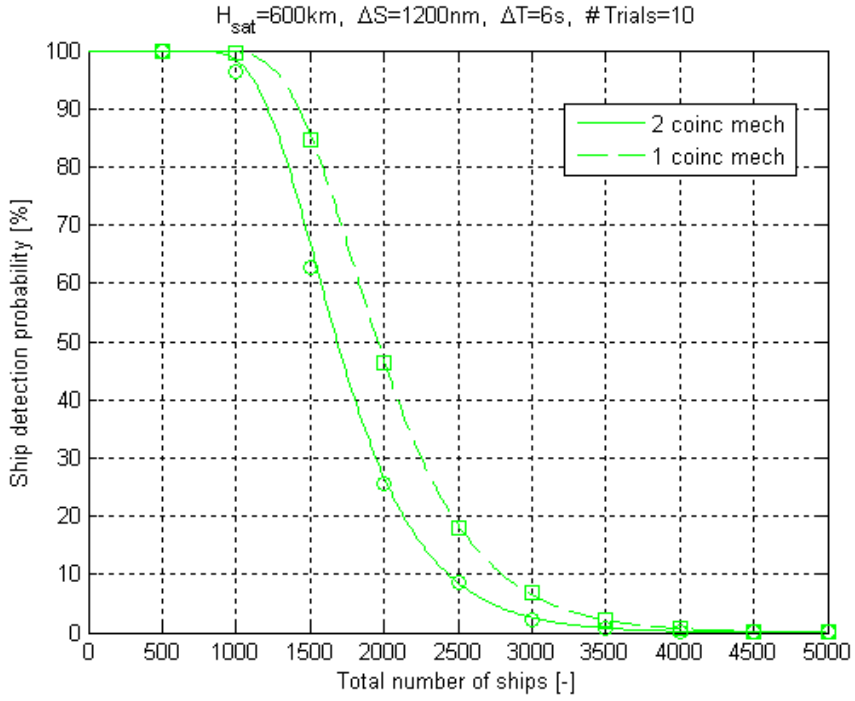

Figure 4.2 *Ship detection probability as a function of total number of ships within the observation area for a 1200 nm wide swath. Circles and squares (2 and 1 coinciding mechanisms) show results from the simulations, while solid and dashed lines show corresponding results from calculations with the nominal ship detection probability equation (3.17)/(3.19).*

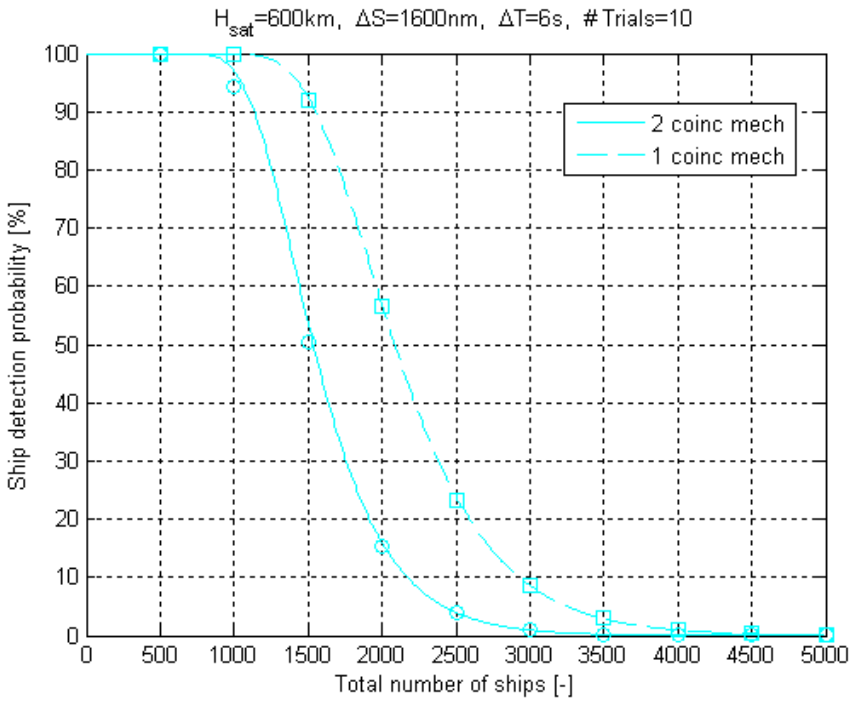

Figure 4.3 *Ship detection probability as a function of total number of ships within the observation area for a 1600 nm wide swath. Circles and squares (2 and 1 coinciding mechanisms) show results from the simulations, while solid and dashed lines show corresponding results from calculations with the nominal ship detection probability equation (3.17)/(3.19).*

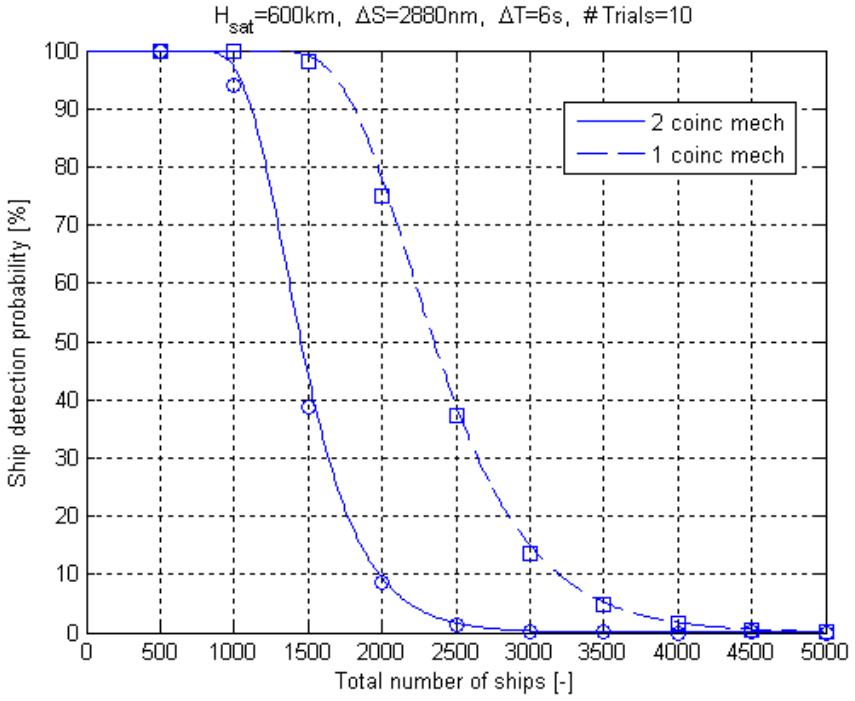

Figure 4.4 *Ship detection probability as a function of total number of ships within the observation area for a 2880 nm wide swath. Circles and squares (2 and 1 coinciding mechanisms) show results from the simulations, while solid and dashed lines show corresponding results from calculations with the nominal ship detection probability equation (3.17)/(3.19).*

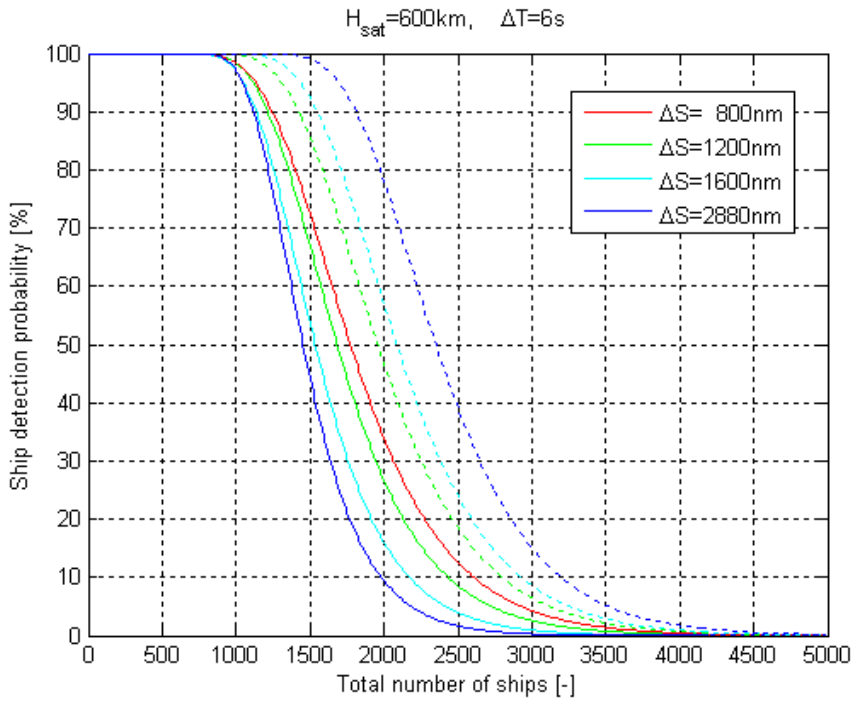

Figure 4.5 *Ship detection probability as a function of total number of ships within the observation area for different swaths. The nominal ship detection probability equation (3.17) (solid line, 2 coinciding mechanisms) and (3.19) (dotted line, 1 coinciding mechanism) was used for the calculations.*

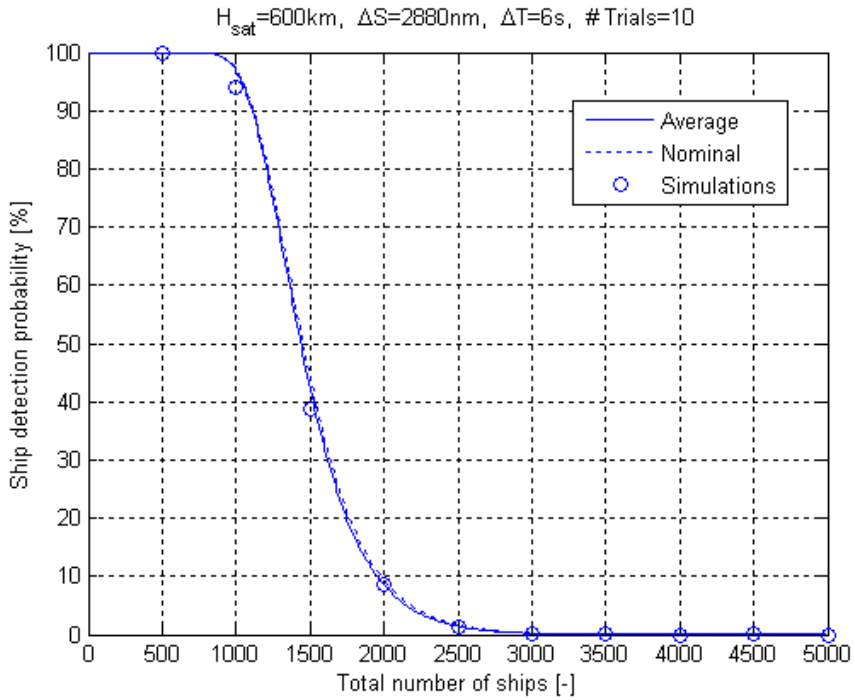

Figure 4.6 *Comparison of the average ship detection probability equation (3.20) with the nominal ship detection probability equation (3.17) and with simulation results.*

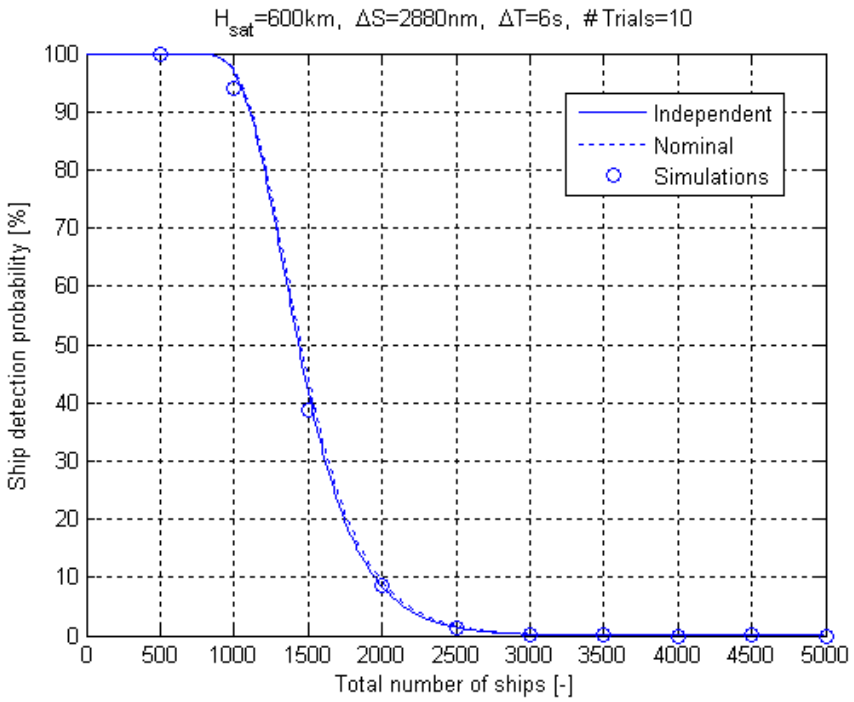

Figure 4.7 *Comparison of the independent ship detection probability equation (3.28) with the nominal ship detection probability equation (3.17) and with simulation results.*

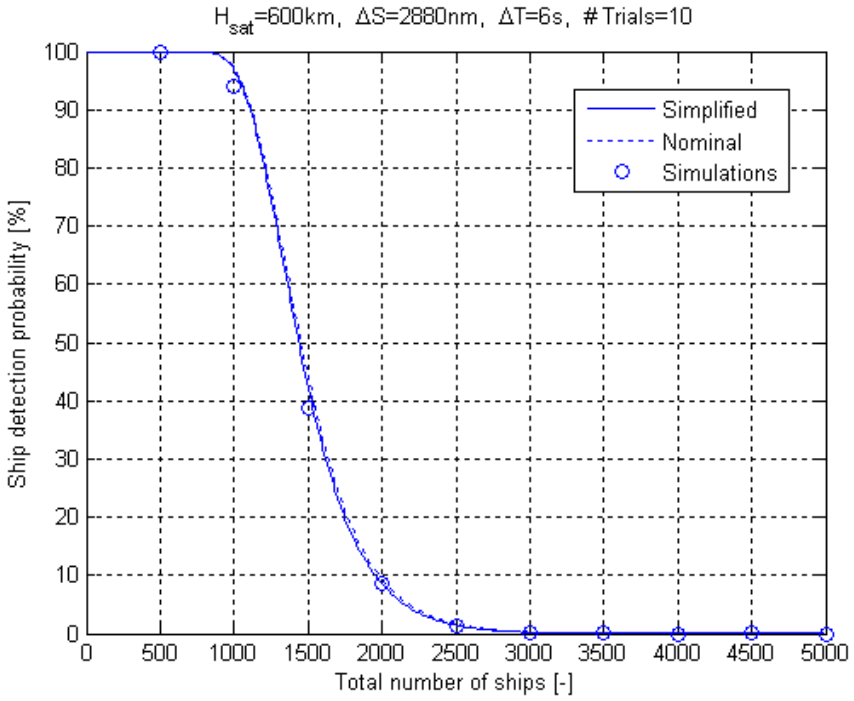

Figure 4.8 *Comparison of the simplified ship detection probability equation (3.33) with the nominal ship detection probability equation (3.17) and with simulation results.*

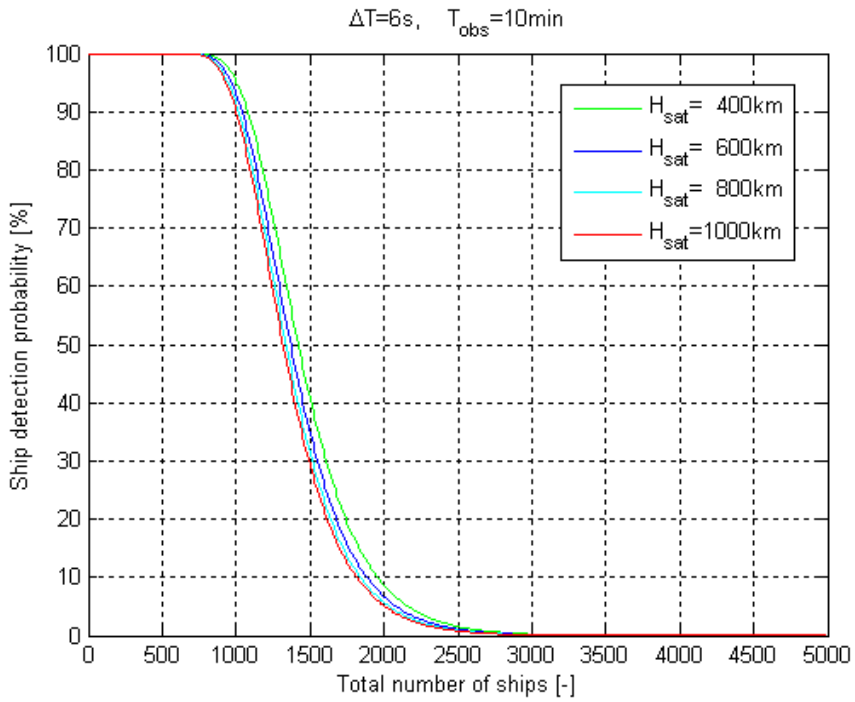

Figure 4.9 *Ship detection probability as a function of total number of ships within the observation area for different AIS sensor altitudes and field of view to the horizon. The observation time is 10 min.*

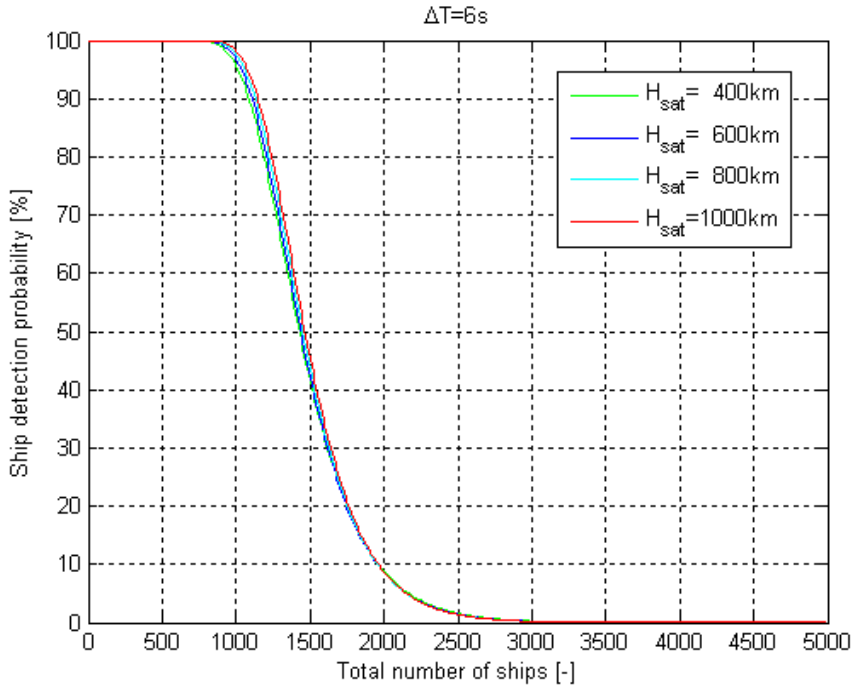

Figure 4.10 *Ship detection probability as a function of total number of ships within the observation area for different AIS sensor altitudes and field of view to the horizon. The observation time varies according to the AIS sensor altitude as given in Table 4.1.*

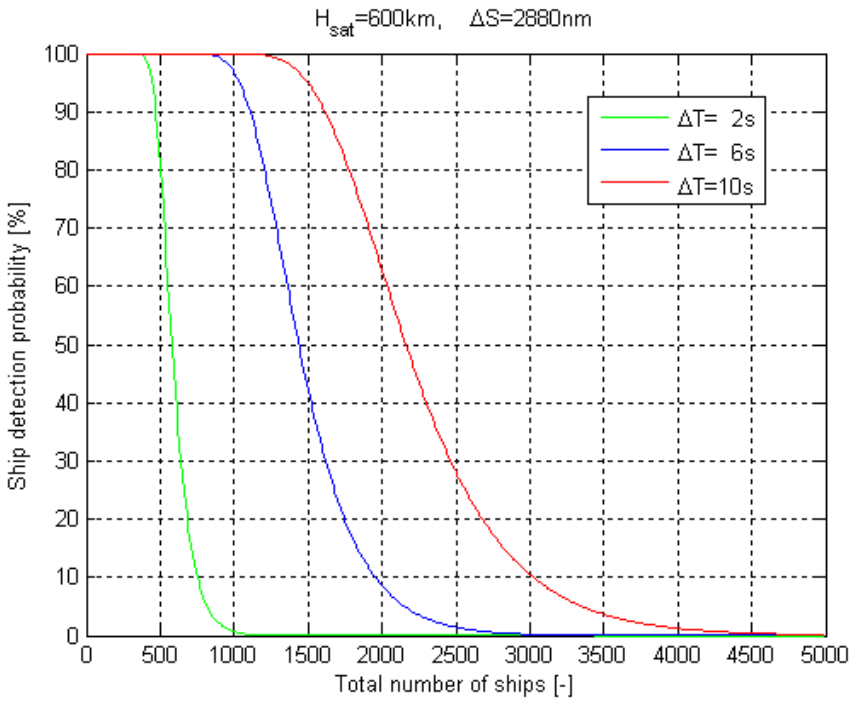

Figure 4.11 Ship detection probability as a function of total number of ships within the observation area for different ship reporting intervals.

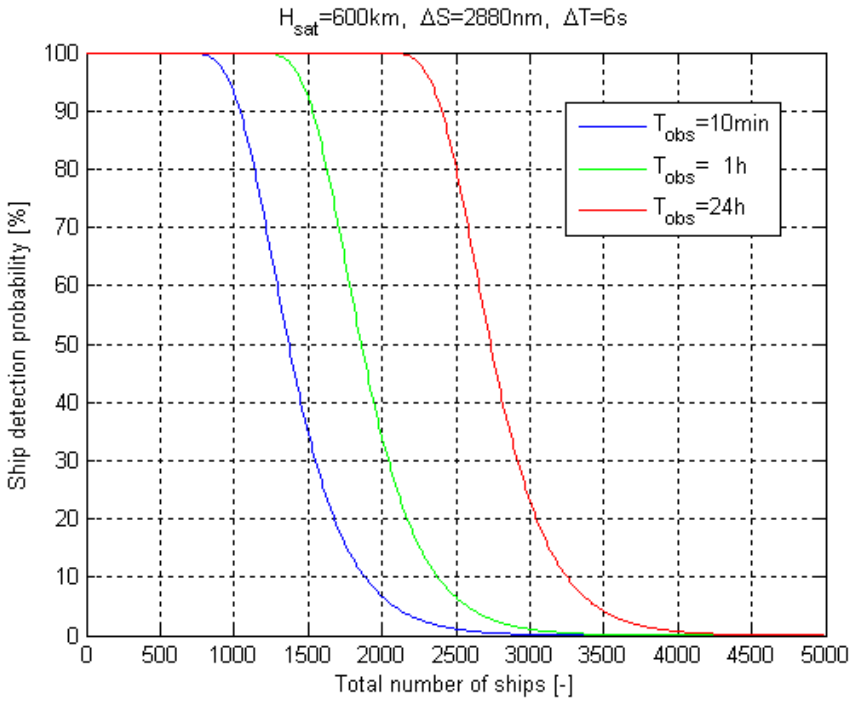

Figure 4.12 Ship detection probability as a function of total number of ships within the observation area for different observation times.

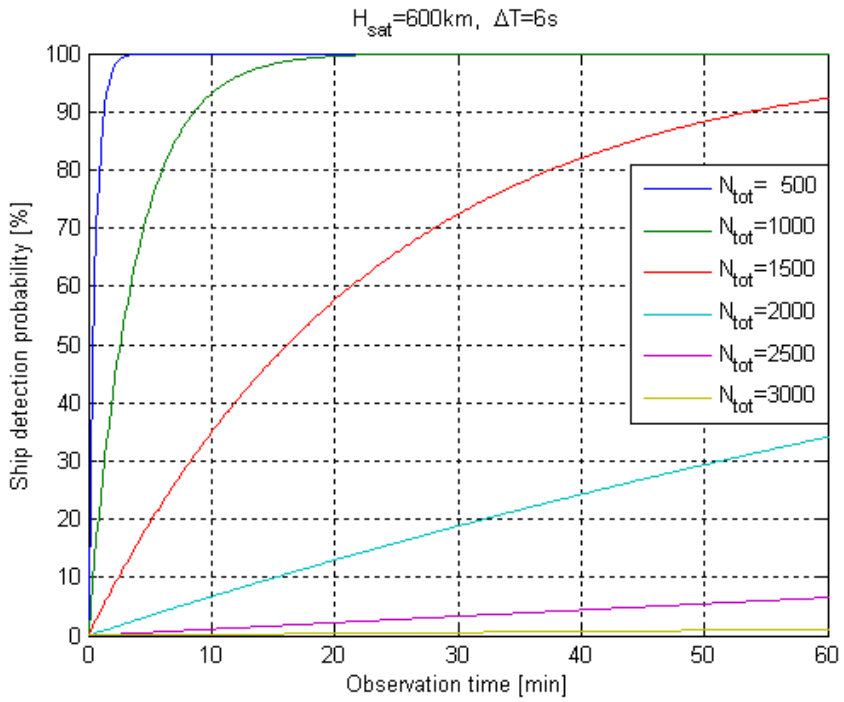

Figure 4.13 *Ship detection probability as a function of observation time (0-60 min) for different numbers of ships within the observation area.*

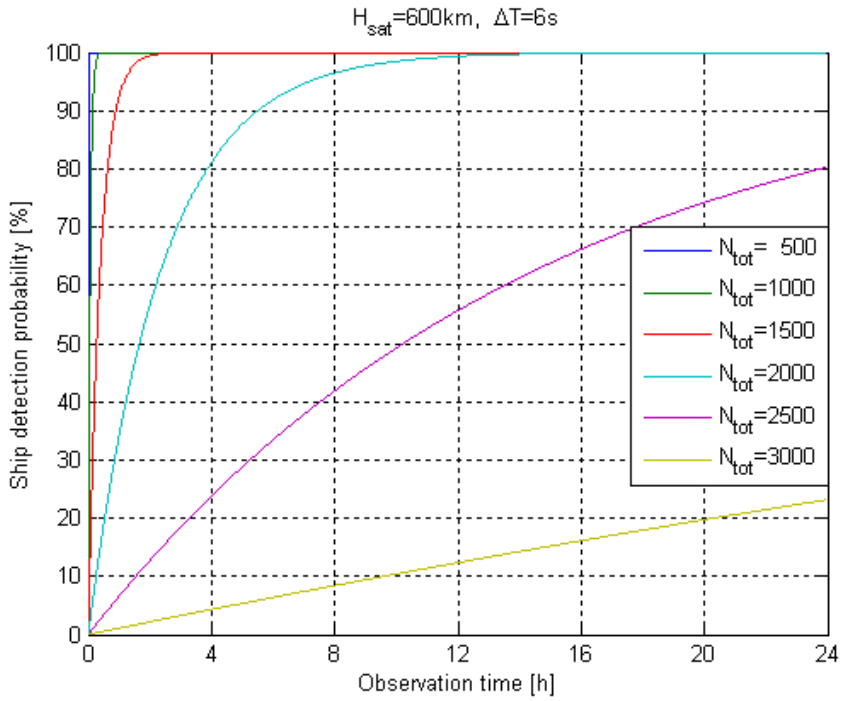

Figure 4.14 *Ship detection probability as a function of observation time (0-24 h) for different numbers of ships within the observation area.*

5 DISCUSSION

We will now discuss the results from the simulations and calculations.

5.1 The ship detection probability equations

First, we want to compare results from the simulations with results from calculations using the analytical expressions for the ship detection probability.

Figure 4.1-Figure 4.4 show the ship detection probability as a function of the total number of ships within the observation area for different swath widths of 800, 1200, 1600, and 2880 nm. Both the simulation results and the results from calculations using the nominal ship detection probability equation (3.17)/(3.19) are shown. The figures show that there is good agreement between the simulations and the nominal ship detection probability equation. There is a difference in the ship detection probability of up to about 5% in the steepest parts of the curve, but there is good agreement in overall shape of the curve and excellent agreement between values for the ship detection probability at both ends of the curve where there is either few ships/high ship detection probability or many ships/low ship detection probability. We conclude that the nominal ship detection probability equation can be used as a good approximation when calculating the ship detection probability for the system.

Figure 4.6 compares the *average* ship detection probability equation (3.20) with the nominal ship detection probability equation and simulations. The figure shows that there is excellent agreement between the two curves and also good agreement with the simulations.

Figure 4.7 compares the *independent* ship detection probability equation (3.28) with the nominal ship detection probability equation and simulations. The figure shows that there is excellent agreement between the two curves and also good agreement with the simulations.

Figure 4.8 compares the *simplified* ship detection probability equation (3.33) with the nominal ship detection probability equation and simulations. The figure shows that there is excellent agreement between the two curves and also good agreement with the simulations.

Both the independent and the simplified ship detection probability equations assume that the ships within the observation area transmit independently of each other. The results, showing good agreement between these two equations and the simulations, confirm that the system in fact can be treated *as if all ships within the observation area transmit independently of each other*. The simplified ship detection probability equation can therefore be used as a good approximation when evaluating the space-based AIS system performance.

5.2 The effect of coinciding transmissions

We want to study the effect of including both mechanisms for coinciding transmissions (see Section 3.1.4) in the calculations.

Figure 4.1-Figure 4.4 show the ship detection probability as a function of the total number of ships within the observation area for different swath widths of 800, 1200, 1600, and 2880 nm. For a swath width of 800 nm (Figure 4.1) the ship detection probability curve that includes two mechanisms for coinciding transmissions is identical to the curve that includes only one mechanism. This is as expected since the second mechanism for coinciding transmissions only enter into effect for swath widths larger than 800 nm (see Section 3.1.4).

When the swath width increases to 1200 nm (Figure 4.2) the two curves start to split. With 1500 ships within the field of view, the first curve (both mechanisms included) gives a ship detection probability of 67%, while the second curve (only one mechanism included) gives a ship detection probability of 85%, i.e., the difference between the two curves is 18%. For a swath width of 1600 nm (Figure 4.3) the curves split further, giving ship detection probabilities of 54% and 93% respectively. With an AIS sensor field of view to the horizon and a swath width of 2880 nm (Figure 4.4) the difference in ship detection probability for the two curves is more than 50% when there are 1500 ships within the field of view. Note that the difference between the two curves is largest in the steep parts of the curves, while approaching zero at both ends of the curves where there is either few ships/high ship detection probability or many ships/low ship detection probability. The ship detection probability curve that includes only one mechanism for coinciding transmissions always gives higher ship detection probability for the same number of ships than the curve that includes both mechanisms.

Figure 4.5 shows curves that include one and two mechanisms for coinciding transmissions for all four swath widths in the same figure. We see that when only one coinciding mechanism is included in the calculations, the ship detection probability *increases* with *increasing* swath width for a given number of ships within the field of view. The reason for this is that increasing the swath width increases the observation time which increases the ship detection probability (see Section 5.5).

When both mechanisms for coinciding transmissions are included in the calculations, two factors with opposite effect come into play:

1. Increasing swath width
   -> increasing observation time
   -> *increasing* ship detection probability
2. Increasing swath width
   -> stronger impact of the second mechanism for coinciding transmissions
   -> *decreasing* ship detection probability

The analyses have shown that the second factor will dominate, and as a result the ship detection probability *decreases* when the swath width *increases* when both mechanisms for coinciding transmissions are included in the calculations.

We conclude that for swath widths up to 800 nm (where only one mechanism for coinciding transmissions is effective) the ship detection probability *increases* with increasing swath width (for given number of ships), while for swath widths larger than 800 nm (where both mechanisms for coinciding transmissions are effective) the ship detection probability *decreases* with increasing swath width. The numbers are valid for an AIS sensor at 600 km altitude.

5.3 AIS sensor altitude

Figure 4.9 shows the ship detection probability as a function of the total number of ships within the observation area for different AIS sensor altitudes of 400, 600, 800, and 1000 km. In each case, the AIS sensor has a field of view to the horizon. This corresponds to swath widths of 2400, 2880, 3280, and 3600 nm respectively. The observation time was set to 10 min.

Figure 4.9 shows that *increasing* the AIS sensor altitude *decreases* the ship detection probability for given number of ships within the field of view when the observation time is constant. The reason for this is that increasing the AIS sensor altitude increases the swath width. This gives a stronger impact of the second mechanism for coinciding transmissions which decreases the ship detection probability. However, the effect is not large. It amounts to a maximum of about 10% difference in the ship detection probability in the steep parts of the curves for the lowest (400 km) and the highest (1000 km) AIS sensor altitude.

Figure 4.10 shows similar curves, but here the observation times have been set according to the swath width, see Table 4.1 for values. In this case, two factors with opposite effect come into play:

1. Increasing swath width (due to increasing AIS sensor altitude)
   -> increasing observation time
   -> *increasing* ship detection probability
2. Increasing swath width (due to increasing AIS sensor altitude)
   -> stronger impact of the second mechanism for coinciding transmissions
   -> *decreasing* ship detection probability

Figure 4.10 shows that these two effects almost cancel each other so that the ship detection probability in fact remains *constant* for *increasing* AIS sensor altitude for given number of ships within the field of view. In reality, there is a slight increase in the ship detection probability for increasing AIS sensor altitude at the steep parts of the curves, but the effect is so small that it is negligible for all practical purposes.

We conclude that varying the altitude (within the range 400-1000 km) for an AIS sensor with field of view to the horizon does not affect the ship detection probability if the number of ships is constant. Note, however, that *increasing* the AIS sensor altitude increases the field of view. The number of ships will therefore normally also increase, and the total effect will be a *decrease* in the ship detection probability.

5.4 Ship reporting interval

Figure 4.11 shows the ship detection probability as a function of the total number of ships within the observation area for different ship reporting intervals of 2, 6, and 10 s. The figure shows that *increasing* the ship reporting interval *increases* the ship detection probability and the number of ships that the system can handle. If requiring a ship detection probability of 99%, the system can handle about 400 ships when the ship reporting interval is 2 s. This number increases to 900 ships if the ship reporting interval is 6 s and to about 1300 ships if the ship reporting interval is 10 s.

5.5 Observation time

Figure 4.12 shows the ship detection probability as a function of the number of ships within the observation area for different observation times of 10 min, 1 h, and 24 h. The figure shows that *increasing* the observation time *increases* the ship detection probability and the number of ships that the system can handle. If requiring a ship detection probability of 99%, the system can handle about 800 ships when the observation time is 10 min. This number increases to 1300 ships if the observation time is 1 h and to about 2200 ships if the observation time is 24 h.

Figure 4.13 and Figure 4.14 show the ship detection probability as a function of observation time for different numbers of ships within the observation area. Curves are shown for 500, 1000, 1500, 2000, 2500, and 3000 ships. Figure 4.13 shows that for relatively low numbers of ships within the observation area (less than 1000 ships) the ship detection probability reaches 90% after less than 10 min. However, for larger number of ships (>2500 ships) the ship detection probability is less than 10% after 1 h. Figure 4.14 shows the ship detection probability for observation times up to 24 h. The figure shows that for up to 2000 ships within the observation area the ship detection probability is better than 99% after 12 h, while for 2500 ships the ship detection probability reaches only 80% after 24 h. For 3000 ships within the observation area the ship detection probability is still less than 25% after 24 h.

We conclude that if an update rate of twice per day is sufficient, the space-based AIS system could handle up to 2000 ships with a ship detection probability of better than 99%. This would, however, require a global constellation of AIS sensors. On the other hand, a single AIS sensor could handle up to about 900 ships within the field of view with a ship detection probability of better than 99% (see Figure 4.11). The update rate in this case would depend on the choice of orbit for the AIS sensor and the latitude of the observation area.

5.6 Summary

The analyses have shown that the space-based AIS system can be treated as if all ships transmit independently of each other. The simplified ship detection probability equation can be used as a good approximation when evaluating the system performance.

We have seen that *increasing* the ship reporting interval and/or the observation time *increases* the ship detection probability and the number of ships that the system can handle. *Increasing* the altitude of an AIS sensor with field of view to the horizon, on the other hand, will normally *decrease* the ship detection probability due to a larger number of ships within the field of view.

The analyses have shown that the ship detection probability *increases* with increasing swath width (for given number of ships) for swath widths up to 800 nm. For swath widths larger than 800 nm the ship detection probability *decreases* with increasing swath width.

Finally, we have seen that a single AIS sensor could handle up to 900 ships within the field of view with a ship detection probability of better than 99%. A global constellation of AIS sensors could handle up to 2000 ships with an update rate of twice per day.

6 SUMMARY

The Universal Shipborne Automatic Identification System (AIS) is a ship-to-ship and ship-to-shore reporting system based on broadcasting of short messages in the maritime VHF band. The AIS messages could possibly also be received from space, and the performance of such a space-based AIS system with respect to ship detection probability has been evaluated in this report. The report continued the work of a previous report (1) that studied the ship detection probability for a space-based AIS system for swath widths up to 800 nm. The present report has extended the analyses to include also fields of view to the horizon.

An observation model for the space-based AIS system was developed for the simulations. Analytical expressions for the ship detection probability were also derived. We found that the ship detection probability P, as a good approximation, can be expressed as

$$P = 1 - \left[1 - \exp\left(-\frac{(1+s) \cdot N_{tot}}{37.5 \cdot n_{ch} \cdot \Delta T} \right) \right]^{\frac{T_{obs}}{\Delta T}} \tag{6.1}$$

where N_{tot} is the total number of ships within the observation area, ΔT is the ship reporting interval, T_{obs} is the observation time, n_{ch} is the number of independent channels used for the transmissions, and s is the overlap factor which value depends on the AIS sensor's altitude and field of view. The equation is valid for all AIS sensor altitudes and all swath widths.

Based on the analyses we found that a single AIS sensor in Low Earth Orbit could handle up to 900 ships within the field of view with a ship detection probability of better than 99%. A global constellation of AIS sensors could handle up to 2000 ships with an update rate of twice per day.

A TABLES

A.1 Swath width and observation time

Frame #*l*	Swath width, Δ*S* (nm)	Swath width, Δ*S* (km)	# Org areas, *M*	Observation time, T_{obs} (s) H_{sat}=400km	H_{sat}=600km	H_{sat}=800km	H_{sat}=1000km
1	80	148	4	21	21	22	23
2	160	296	16	41	43	45	47
3	240	444	36	62	64	67	70
4	320	592	64	82	86	90	93
5	400	740	100	103	107	112	117
6	480	888	144	123	129	135	140
7	560	1036	196	144	150	157	163
8	640	1184	256	164	172	179	186
9	720	1332	324	185	193	202	210
10	800	1480	400	206	214	224	233
11	880	1628	484	226	236	247	256
12	960	1776	576	247	257	269	280
13	1040	1924	676	267	279	292	303
14	1120	2072	784	288	300	314	326
15	1200	2220	900	308	322	336	350
16	1280	2368	1024	329	343	359	373
17	1360	2516	1156	349	365	381	396
18	1440	2664	1296	370	386	404	420
19	1520	2812	1444	391	408	426	443
20	1600	2960	1600	411	429	448	466
21	1680	3108	1764	432	450	471	489
22	1760	3256	1936	452	472	493	513
23	1840	3404	2116	473	493	516	356
24	1920	3552	2304	493	515	538	559
25	2000	3700	2500	514	536	561	583
26	2080	3848	2704	534	558	583	606
27	2160	3996	2916	555	579	605	629
28	2240	4144	3136	576	601	628	653
29	2320	4292	3364	596	622	650	676
30	2400	4440	3600	617	643	673	699

Table continues on next page

Table continued from previous page

Frame #l	Swath width, ΔS		# Org areas, M	Observation time, T_{obs} (s)			
	(nm)	(km)		H_{sat}=400km	H_{sat}=600km	H_{sat}=800km	H_{sat}=1000km
31	2480	4588	3844	-	665	695	723
32	2560	4736	4096	-	686	718	746
33	2640	4884	4356	-	708	740	769
34	2720	5032	4624	-	729	762	792
35	2800	5180	4900	-	751	785	816
36	2880	5328	5184	-	772	807	839
37	2960	5476	5476	-	-	830	862
38	3040	5624	5776	-	-	852	886
39	3120	5772	6084	-	-	875	909
40	3200	5920	6400	-	-	897	932
41	3280	6068	6724	-	-	919	956
42	3360	6216	7056	-	-	-	979
43	3440	6364	7396	-	-	-	1002
44	3520	6512	7744	-	-	-	1026
45	3600	6660	8100	-	-	-	1049

Table A.1 Corresponding values for frame, swath width ΔS, number of organized areas M, and observation times T_{obs} for different AIS sensor altitudes. Note that only the observation times depend on the AIS sensor altitude.

A.2 Ground range and organized areas

Frame #l	Ground range, R_g		Org area #m	# Org areas in frame, M^l
	(nm)	(km)		
1	0	0	1-4	4
2	40	74	5-16	12
3	80	148	17-36	20
4	120	222	37-64	28
5	160	296	65-100	36
6	200	370	101-144	44
7	240	444	145-196	52
8	280	518	197-256	60
9	320	592	257-324	68
10	360	666	325-400	76
11	400	740	401-484	84
12	440	814	485-576	92
13	480	888	577-676	100
14	520	962	677-784	108
15	560	1036	785-900	116
16	600	1110	901-1024	124
17	640	1184	1025-1156	132
18	680	1258	1157-1296	140
19	720	1332	1297-1444	148
20	760	1406	1445-1600	156
21	800	1480	1601-1764	164
22	840	1554	1765-1936	172
23	880	1628	1937-2116	180
24	920	1702	2117-2304	188
25	960	1776	2305-2500	196
26	1000	1850	2501-2704	204
27	1040	1924	2705-2916	212
28	1080	1998	2917-3136	220
29	1120	2072	3137-3364	228
30	1160	2146	3365-3600	236

Table continues on next page

Table continued from previous page

Frame	**Ground range, R_g**		**Org area**	**# Org areas in**
#l	**(nm)**	**(km)**	***#m***	**frame, M^l**
31	1200	2220	3601-3844	244
32	1240	2294	3845-4096	252
33	1280	2368	4097-4356	260
34	1320	2442	4357-4624	268
35	1360	2516	4625-4900	276
36	1400	2590	4901-5184	284
37	1440	2664	5185-5476	292
38	1480	2738	5477-5776	300
39	1520	2812	5777-6084	308
40	1560	2886	6085-6400	316
41	1600	2960	6401-6724	324
42	1640	3034	6725-7056	332
43	1680	3108	7057-7396	340
44	1720	3182	7397-7744	348
45	1760	3256	7745-8100	356

Table A.2 *Corresponding values for frame #l that marks the outer border of the observation area, ground range R_g, the numbers for the organized areas in frame #l, and the total number of organized areas M^l in frame #l. All values in the table are independent of the AIS sensor altitude.*

A.3 Slant range and distribution of main areas

A.3.1 AIS sensor altitude of 400 km

Frame #*l*	Slant range, R_s		Main area (I)		Main area (IIa)		Main area (IIb)		M_I^l	M_{II}^l
	(nm)	(km)	$_{min}L_I^l$	$_{max}L_I^l$	$_{min}L_{IIa}^l$	$_{max}L_{IIa}^l$	$_{min}L_{IIb}^l$	$_{max}L_{IIb}^l$		
1	216	400	1	9	-	-	10	30	324	3276
2	220	407	1	9	-	-	10	30	324	3276
3	231	428	1	10	-	-	11	30	400	3200
4	249	461	1	10	-	-	11	30	400	3200
5	272	503	1	11	-	-	12	30	484	3116
6	299	553	1	11	-	-	12	30	484	3116
7	329	608	1	12	-	-	13	30	576	3024
8	361	667	1	13	-	-	14	30	676	2924
9	395	730	1	14	-	-	15	30	784	2816
10	429	794	3	15	1	2	16	30	884	2716
11	465	861	5	16	1	4	17	30	960	2640
12	502	929	7	17	1	6	18	30	1012	2588
13	539	998	8	18	1	7	19	30	1100	2500
14	577	1068	9	19	1	8	20	30	1188	2412
15	616	1139	10	20	1	9	21	30	1276	2324
16	655	1211	11	21	1	10	22	30	1364	2236
17	694	1283	12	22	1	11	23	30	1452	2148
18	732	1355	13	23	1	12	24	30	1540	2060
19	772	1428	14	24	1	13	25	30	1628	1972
20	811	1501	15	25	1	14	26	30	1716	1884
21	851	1574	16	26	1	15	27	30	1804	1796
22	890	1647	17	27	1	16	28	30	1892	1708
23	930	1721	18	28	1	17	29	30	1980	1620
24	970	1795	19	29	1	18	30	30	2068	1532
25	1010	1868	20	30	1	19	-	-	2156	1444
26	1050	1942	21	30	1	20	-	-	2000	1600
27	1090	2016	22	30	1	21	-	-	1836	1764
28	1130	2090	23	30	1	22	-	-	1664	1936
29	1170	2164	24	30	1	23	-	-	1484	2116
30	1210	2238	25	30	1	24	-	-	1296	2304

Table text on next page

Table A.3 *Corresponding values for frame #l, slant range R_s from the AIS sensor to frame #l, minimum and maximum numbers $_{\min}L_I^l$ and $_{\max}L_I^l$ for frames that are placed in main area (I) relative to frame #l, minimum and maximum numbers $_{\min}L_{IIa}^l$ and $_{\max}L_{IIa}^l$ for frames that are placed in main area (IIa) relative to frame #l, minimum and maximum numbers $_{\min}L_{IIb}^l$ and $_{\max}L_{IIb}^l$ for frames that are placed in main area (IIb) relative to frame #l, and the numbers of organized areas M_I^l and M_{II}^l that are placed in main areas (I) and (II) relative to frame #l. The values are valid for an AIS sensor altitude of 400 km. The values for M_I^l and M_{II}^l are valid for a field of view to the horizon (swath width 2400 nm).*

A.3.2 AIS sensor altitude of 600 km

Frame #l	Slant range, R_s		Main area (I)		Main area (IIa)		Main area (IIb)			
	(nm)	(km)	$_{min}L^{l}_{I}$	$_{max}L^{l}_{I}$	$_{min}L^{l}_{IIa}$	$_{max}L^{l}_{IIa}$	$_{min}L^{l}_{IIb}$	$_{max}L^{l}_{IIb}$	M^{l}_{I}	M^{l}_{II}
1	324	600	1	10	-	-	11	36	400	4784
2	327	605	1	10	-	-	11	36	400	4784
3	335	620	1	11	-	-	12	36	484	4700
4	348	643	1	11	-	-	12	36	484	4700
5	365	675	1	12	-	-	13	36	576	4608
6	386	714	1	12	-	-	13	36	576	4608
7	411	759	1	13	-	-	14	36	676	4508
8	437	808	1	14	-	-	15	36	784	4400
9	466	862	1	14	-	-	15	36	784	4400
10	497	919	1	15	-	-	16	36	900	4284
11	529	979	3	16	1	2	17	36	1008	4176
12	563	1041	5	17	1	4	18	36	1092	4092
13	597	1105	7	18	1	6	19	36	1152	4032
14	632	1170	8	19	1	7	20	36	1248	3936
15	669	1238	10	20	1	9	21	36	1276	3908
16	706	1306	11	21	1	10	22	36	1364	3820
17	743	1375	12	22	1	11	23	36	1452	3732
18	781	1444	13	23	1	12	24	36	1540	3644
19	819	1515	14	24	1	13	25	36	1628	3556
20	857	1586	15	25	1	14	26	36	1716	3468
21	896	1657	16	26	1	15	27	36	1804	3380
22	935	1729	17	27	1	16	28	36	1892	3292
23	974	1801	18	28	1	17	29	36	1980	3204
24	1013	1874	19	29	1	18	30	36	2068	3116
25	1052	1946	20	30	1	19	31	36	2156	3028
26	1091	2019	21	31	1	20	32	36	2244	2940
27	1131	2093	22	32	1	21	33	36	2332	2852
28	1171	2166	23	33	1	22	34	36	2420	2764
29	1211	2240	24	34	1	23	35	36	2508	2676
30	1250	2313	25	35	1	24	36	36	2596	2588

Table continues on next page

Table continued from previous page

Frame #l	Slant range, R_s		Main area (I)		Main area (IIa)		Main area (IIb)		M_I^l	M_{II}^l
	(nm)	(km)	$_{\min}L_I^l$	$_{\max}L_I^l$	$_{\min}L_{IIa}^l$	$_{\max}L_{IIa}^l$	$_{\min}L_{IIb}^l$	$_{\max}L_{IIb}^l$		
31	1290	2387	26	36	1	25	-	-	2684	2500
32	1330	2461	27	36	1	26	-	-	2480	2704
33	1370	2535	28	36	1	27	-	-	2268	2916
34	1410	2609	29	36	1	28	-	-	2048	3136
35	1450	2683	30	36	1	29	-	-	1820	3364
36	1490	2757	31	36	1	30	-	-	1584	3600

Table A.4 Corresponding values for frame #l, slant range R_s from the AIS sensor to frame #l, minimum and maximum numbers $_{\min}L_I^l$ and $_{\max}L_I^l$ for frames that are placed in main area (I) relative to frame #l, minimum and maximum numbers $_{\min}L_{IIa}^l$ and $_{\max}L_{IIa}^l$ for frames that are placed in main area (IIa) relative to frame #l, minimum and maximum numbers $_{\min}L_{IIb}^l$ and $_{\max}L_{IIb}^l$ for frames that are placed in main area (IIb) relative to frame #l, and the numbers of organized areas M_I^l and M_{II}^l that are placed in main areas (I) and (II) relative to frame #l. The values are valid for an AIS sensor altitude of 600 km. The values for M_I^l and M_{II}^l are valid for a field of view to the horizon (swath width 2880 nm).

A.3.3 AIS sensor altitude of 800 km

Frame #l	Slant range, R_s		Main area (I)		Main area (IIa)		Main area (IIb)			
	(nm)	(km)	$_{min}L^{l}_{I}$	$_{max}L^{l}_{I}$	$_{min}L^{l}_{IIa}$	$_{max}L^{l}_{IIa}$	$_{min}L^{l}_{IIb}$	$_{max}L^{l}_{IIb}$	M^{l}_{I}	M^{l}_{II}
1	432	800	1	11	-	-	12	41	484	6240
2	435	804	1	11	-	-	12	41	484	6240
3	441	815	1	12	-	-	13	41	576	6148
4	451	834	1	12	-	-	13	41	576	6148
5	464	859	1	12	-	-	13	41	576	6148
6	482	891	1	13	-	-	14	41	676	6048
7	502	928	1	14	-	-	15	41	784	5940
8	524	970	1	14	-	-	15	41	784	5940
9	550	1017	1	15	-	-	16	41	900	5824
10	577	1067	1	16	-	-	17	41	1024	5700
11	606	1121	1	17	-	-	18	41	1156	5568
12	636	1177	3	17	1	2	18	41	1140	5584
13	668	1235	6	18	1	5	19	41	1196	5528
14	701	1296	7	19	1	6	20	41	1300	5424
15	734	1358	9	20	1	8	21	41	1344	5380
16	769	1422	10	21	1	9	22	41	1440	5284
17	804	1488	11	22	1	10	23	41	1536	5188
18	840	1554	13	23	1	12	24	41	1540	5184
19	877	1622	14	24	1	13	25	41	1628	5096
20	914	1690	15	25	1	14	26	41	1716	5008
21	951	1759	16	26	1	15	27	41	1804	4920
22	989	1829	17	27	1	16	28	41	1892	4832
23	1026	1899	18	28	1	17	29	41	1980	4744
24	1065	1970	19	29	1	18	30	41	2068	4656
25	1103	2041	20	30	1	19	31	41	2156	4568
26	1142	2113	21	31	1	20	32	41	2244	4480
27	1181	2185	22	32	1	21	33	41	2332	4392
28	1220	2257	23	33	1	22	34	41	2420	4304
29	1259	2330	24	34	1	23	35	41	2508	4216
30	1299	2403	25	35	1	24	36	41	2596	4128

Table continues on next page

Table continued from previous page

Frame #*l*	Slant range, R_s		Main area (I)		Main area (IIa)		Main area (IIb)		M_I^l	M_{II}^l
	(nm)	(km)	$_{\min}L_I^l$	$_{\max}L_I^l$	$_{\min}L_{IIa}^l$	$_{\max}L_{IIa}^l$	$_{\min}L_{IIb}^l$	$_{\max}L_{IIb}^l$		
31	1338	2476	26	36	1	25	37	41	2684	4040
32	1378	2549	27	37	1	26	38	41	2772	3952
33	1417	2623	28	38	1	27	39	41	2860	3864
34	1457	2696	29	39	1	28	40	41	2948	3776
35	1497	2770	30	40	1	29	41	41	3036	3688
36	1537	2844	31	41	1	30	-	-	3124	3600
37	1577	2917	32	41	1	31	-	-	2880	3844
38	1617	2991	33	41	1	32	-	-	2628	4096
39	1657	3065	34	41	1	33	-	-	2368	4356
40	1697	3139	35	41	1	34	-	-	2100	4626
41	1737	3213	36	41	1	35	-	-	1824	4900

Table A.5 Corresponding values for frame #l, slant range R_s from the AIS sensor to frame #l, minimum and maximum numbers $_{\min}L_I^l$ and $_{\max}L_I^l$ for frames that are placed in main area (I) relative to frame #l, minimum and maximum numbers $_{\min}L_{IIa}^l$ and $_{\max}L_{IIa}^l$ for frames that are placed in main area (IIa) relative to frame #l, minimum and maximum numbers $_{\min}L_{IIb}^l$ and $_{\max}L_{IIb}^l$ for frames that are placed in main area (IIb) relative to frame #l, and the numbers of organized areas M_I^l and M_{II}^l that are placed in main areas (I) and (II) relative to frame #l. The values are valid for an AIS sensor altitude of 800 km. The values for M_I^l and M_{II}^l are valid for a field of view to the horizon (swath width 3280 nm).

A.3.4 AIS sensor altitude of 1000 km

Frame #l	Slant range, R_s		Main area (I)		Main area (IIa)		Main area (IIb)		M_I^l	M_{II}^l
	(nm)	(km)	$_{min}L_I^l$	$_{max}L_I^l$	$_{min}L_{IIa}^l$	$_{max}L_{IIa}^l$	$_{min}L_{IIb}^l$	$_{max}L_{IIb}^l$		
1	541	1000	1	12	-	-	13	45	576	7524
2	542	1003	1	12	-	-	13	45	576	7524
3	548	1013	1	13	-	-	14	45	676	7424
4	556	1028	1	13	-	-	14	45	676	7424
5	567	1049	1	13	-	-	14	45	676	7424
6	582	1076	1	14	-	-	15	45	784	7316
7	599	1108	1	14	-	-	15	45	784	7316
8	619	1145	1	15	-	-	16	45	900	7200
9	641	1185	1	16	-	-	17	45	1024	7076
10	665	1230	1	16	-	-	17	45	1024	7076
11	691	1278	1	17	-	-	18	45	1156	6944
12	718	1329	1	18	-	-	19	45	1296	6804
13	747	1382	3	19	1	2	20	45	1428	6672
14	777	1438	5	19	1	4	20	45	1380	6720
15	809	1496	7	20	1	6	21	45	1456	6644
16	841	1556	9	21	1	8	22	45	1508	6592
17	875	1618	10	22	1	9	23	45	1612	6488
18	909	1681	12	23	1	11	24	45	1632	6468
19	943	1745	13	24	1	12	25	45	1728	6372
20	978	1810	15	25	1	14	26	45	1716	6384
21	1015	1877	16	26	1	15	27	45	1804	6296
22	1051	1944	17	27	1	16	28	45	1892	6208
23	1088	2013	18	28	1	17	29	45	1980	6120
24	1125	2081	19	29	1	18	30	45	2068	6032
25	1163	2151	20	30	1	19	31	45	2156	5944
26	1201	2221	21	31	1	20	32	45	2244	5856
27	1238	2291	22	32	1	21	33	45	2332	5768
28	1277	2362	23	33	1	22	34	45	2420	5680
29	1316	2434	24	34	1	23	35	45	2508	5592
30	1354	2505	25	35	1	24	36	45	2596	5504

Table continues on next page

Table continued from previous page

Frame #*l*	Slant range, R_s		Main area (I)		Main area (IIa)		Main area (IIb)		M_I^l	M_{II}^l
	(nm)	(km)	$\min L_I^l$	$\max L_I^l$	$\min L_{IIa}^l$	$\max L_{IIa}^l$	$\min L_{IIb}^l$	$\max L_{IIb}^l$		
31	1394	2578	26	36	1	25	37	45	2684	5416
32	1432	2650	27	37	1	26	38	45	2772	5328
33	1472	2723	28	38	1	27	39	45	2860	5240
34	1511	2795	29	39	1	28	40	45	2948	5152
35	1551	2869	30	40	1	29	41	45	3036	5064
36	1590	2942	31	41	1	30	42	45	3124	4976
37	1630	3015	32	42	1	31	43	45	3212	4888
38	1670	3089	33	43	1	32	44	45	3300	4800
39	1709	3162	34	44	1	33	45	45	3388	4712
40	1749	3236	35	45	1	34	-	-	3476	4624
41	1789	3310	36	45	1	35	-	-	3200	4900
42	1829	3384	37	45	1	36	-	-	2916	5184
43	1869	3458	38	45	1	37	-	-	2624	5476
44	1909	3532	39	45	1	38	-	-	2324	5776
45	1949	3606	40	45	1	39	-	-	2016	6084

Table A.6 Corresponding values for frame #l, slant range R_s from the AIS sensor to frame #l, minimum and maximum numbers $\min L_I^l$ and $\max L_I^l$ for frames that are placed in main area (I) relative to frame #l, minimum and maximum numbers $\min L_{IIa}^l$ and $\max L_{IIa}^l$ for frames that are placed in main area (IIa) relative to frame #l, minimum and maximum numbers $\min L_{IIb}^l$ and $\max L_{IIb}^l$ for frames that are placed in main area (IIb) relative to frame #l, and the numbers of organized areas M_I^l and M_{II}^l that are placed in main areas (I) and (II) relative to frame #l. The values are valid for an AIS sensor altitude of 1000 km. The values for M_I^l and M_{II}^l are valid for a field of view to the horizon (swath width 3600 nm).

A.4 Average values for the ship distribution in the main areas

H_{sat} (km)	M_I	M_{II}	M	s
400	1527	2073	3600	0.5759
600	1886	3298	5184	0.6362
800	2189	4535	6724	0.6744
1000	2436	5664	8100	0.6992

Table A.7 Corresponding values for AIS sensor altitude H_{sat}, average numbers $\bar{M}_I$ and $\bar{M}_{II}$ of organized areas in main areas (I) and (II), total number of organized areas M within the observation area, and the overlap factor s. The values are valid for an AIS sensor field of view to the horizon.

B THE FILL FACTOR, *K*

The AIS messages are entered into a 1 minute long message frame of 2250 message slots. We assume that one AIS message occupies exactly one message slot. If the AIS messages from two different ships are sent in the same message slot, both AIS messages will be lost.

A distance delay buffer in the AIS standard prevents AIS messages that are sent in adjacent message slots from being received simultaneously at the AIS sensor as long as the difference in signal path length is less than about 200 nm (see Section 3.1.4). Ships that are placed in such a way relative to the ship being observed that this is true, is said to be in main area (I) (see Section 3.2). An example of the message frame for an organized area in main area (I) is shown in Figure B.1 (upper part). The figure shows the message frame *relative* to the ship being observed.

For differences in the signal path lengths that are larger than about 200 nm the distance delay buffer is not sufficient, and messages sent in adjacent message slots will overlap. Ships that are placed such that this is true is said to be in main area (IIa) or (IIb) relative to the ship being observed. This situation is illustrated in Figure B.1 (lower part).

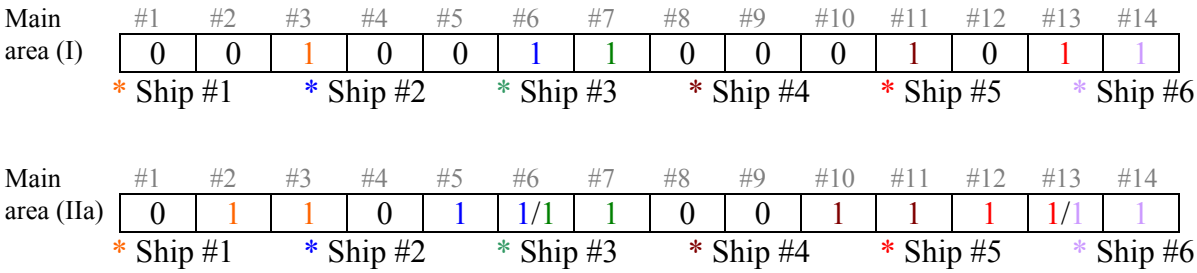

Figure B.1 The message frames for an organized area when the organized area is placed in main area (I) (upper part) and main area (IIa) (lower part) respectively.

The fill factor k describes how "filled up" the message frame for an organized area is as seen from the ship being observed. The fill factor depends on the fraction of ships $N / N_{\max}$ in the organized area

$$k = k\left(\frac{N}{N_{\max}}\right) \tag{B.1}$$

where N is the number of ships and $N_{\max}$ is the maximum possible number of ships within the organized area.

When the ships are placed in main area (I) relative to the ship being observed (as illustrated in the upper part of Figure B.1), the fill factor is by definition

$$k = 1 \tag{B.2}$$

i.e., each message occupies exactly one slot.

When the ships are placed in main area (IIa) or (IIb) relative to the ship being observed, the fill factor is

$$1 \le k \le 2 \tag{B.3}$$

The value of k for this case depends on the fraction $N / N_{\max}$, that is, it depends on how "filled up" with ships the organized area is. If the organized area is almost empty ($N / N_{\max} \ll 1$)

$$k \to 2 \tag{B.4}$$

The reason for this is that in this case each message will be seen to occupy 2 message slots (as is the case for the messages from ships #1 and #4 in the message frame for main area (IIa) in the lower part of Figure B.1).

However, if the organized area is almost filled up with ships ($N \to N_{\max}$)

$$k \to 1 \tag{B.5}$$

The reason for this is that in this case there are almost no extra empty message slots to occupy (messages from ships #2 and #3 in the message frame for main area (IIa) in the lower part of Figure B.1 do, for instance, "share" one message slot).

Simulations were performed to determine the fill factor k as a function of the fraction of ships $N / N_{\max}$. We found that the fill factor as a good approximation can be written as

$$k = 2 - \frac{N}{N_{\max}} \tag{B.6}$$

Equation (B.6) is valid for main area (II).

Results from the simulations and calculations with Equation (B.6) are compared in Figure B.2, and show that Equation (B.6) can be used as a good approximation.

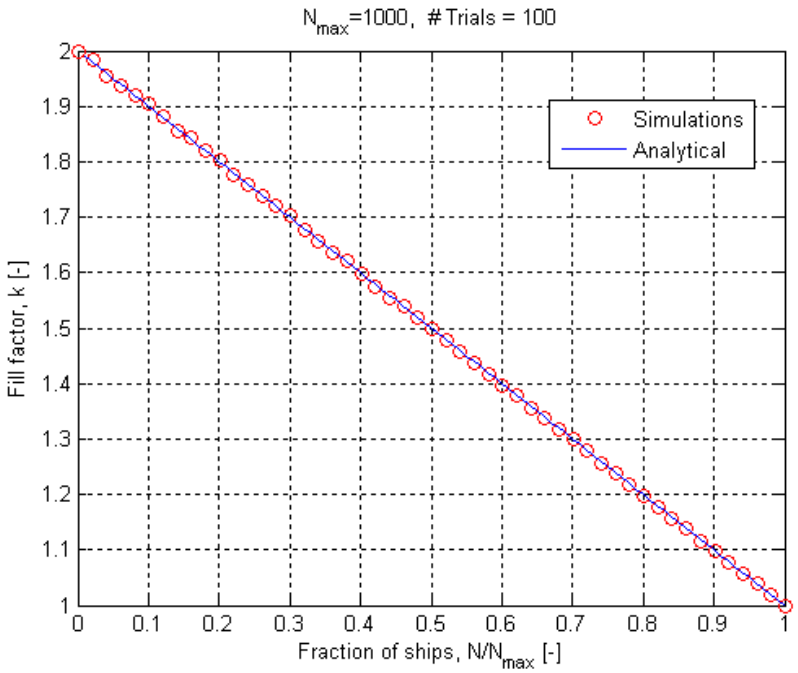

Figure B.2 The fill factor k. Results from simulations (red circles) are shown together with results from calculations with Equation B.6 (blue solid line).

References

(1) HØYE Gudrun (2004): (U)Observation modelling and detection probability for space-based AIS reception, FFI/RAPPORT-2004/01113, RESTRICTED.

(2) IMO (1974/1980): "International convention for the Safety of Life at Sea (SOLAS)" - Chapter V "Safety of Navigation" - Regulation 19.

(3) ITU, Recommendation, ITU-R M.1371 (2001): "Technical Characteristics for a Universal Shipborne Automatic Identification System using Time Division Multiple Access in the VHF Maritime Mobile Band".

(4) S Barnett and T M Cronin (1986): Mathematical Formulae, Prentice-Hall.

(5) HØYE Gudrun (2008): A simulation program for ship detection probability analyses for space-based AIS, FFI-notat 2008/00158, In Confidence.